https://ntrs.nasa.gov/search.jsp?R=19870017022 2020-03-20T09:50:07+00:00Z

IN-44
87060
31P.

DOE/NASA/20320-72
NASA TM-89903

Surface Pressure Measurements on the Blade of an Operating Mod-2 Wind Turbine With and Without Vortex Generators

(NASA-TM-89903) SURFACE PRESSURE MEASUREMENTS ON THE BLADE OF AN OPERATING MOD-2 WIND TURBINE WITH AND WITHOUT VORTEX GENERATORS (NASA) 37 p Avail: NTIS HC A03/MF A01 CSCL 10A G3/44

N87-26455

Unclas
0087060

Ted W. Nyland
National Aeronautics and Space Administration
Lewis Research Center

August 1987

Prepared for
U.S. DEPARTMENT OF ENERGY
Conservation and Renewable Energy
Wind/Ocean Technology Division

DISCLAIMER

This report was prepared as an account of work sponsored by an agency of the United States Government. Neither the United States Government nor any agency thereof, nor any of their employees, makes any warranty, express or implied, or assumes any legal liability or responsibility for the accuracy, completeness, or usefulness of any information, apparatus, product, or process disclosed, or represents that its use would not infringe privately owned rights. Reference herein to any specific commercial product, process, or service by trade name, trademark, manufacturer, or otherwise, does not necessarily constitute or imply its endorsement, recommendation, or favoring by the United States Government or any agency thereof. The views and opinions of authors expressed herein do not necessarily state or reflect those of the United States Government or any agency thereof.

Printed in the United States of America

Available from
National Technical Information Service
U.S. Department of Commerce
5285 Port Royal Road
Springfield, VA 22161

NTIS price codes[1]
Printed copy: A03
Microfiche copy: A01

[1]Codes are used for pricing all publications. The code is determined by the number of pages in the publication. Information pertaining to the pricing codes can be found in the current issues of the following publications, which are generally available in most libraries: *Energy Research Abstracts (ERA); Government Reports Announcements* and Index (*GRA* and I); *Scientific and Technical Abstract Reports (STAR);* and publication, NTIS-PR-360 available from NTIS at the above address.

DOE/NASA/20320-72
NASA TM-89903

Surface Pressure Measurements on the Blade of an Operating Mod-2 Wind Turbine With and Without Vortex Generators

Ted W. Nyland
National Aeronautics and Space Administration
Lewis Research Center
Cleveland, Ohio 44135

August 1987

Work performed for
U.S. DEPARTMENT OF ENERGY
Conservation and Renewable Energy
Wind/Ocean Technology Division
Washington, D.C. 20545
Under Interagency Agreement DE-AI01-76ET20320

SURFACE PRESSURE MEASUREMENTS ON THE BLADE OF AN OPERATING MOD-2 WIND TURBINE WITH AND WITHOUT VORTEX GENERATORS

Ted W. Nyland
National Aeronautics and Space Administration
Lewis Research Center
Cleveland, Ohio 44135

SUMMARY

Pressure measurements covering a range of wind velocities were made at one span location on the surface of an operating Mod-2, 2500-kW, wind turbine blade. The data, which were taken with and without vortex generators installed on the leading edge, show the existence of higher pressure coefficients than would be expected from two-dimensional wind tunnel data. These high pressure ratios may be the result of three-dimensional flow over the blade, which delays flow separation. Data are presented showing the repetitiveness of abrupt changes in the pressure distribution that occur as the blade rotates. Calculated values of suction and flap coefficients are also presented.

INTRODUCTION

Experience has shown that the performance (i.e., output power as a function of wind speed) of propeller-type wind turbine rotors operating in the fixed-pitch mode cannot be accurately predicted at high wind speeds (ref. 1). Computer codes, based on two-dimensional blade-element momentum theory, predict that the rotor output power will increase with wind speed until a peak is reached, and then will drop off rapidly as the wind speed continues to rise. The codes make use of two-dimensional, wind tunnel measured lift and drag coefficients. This dropoff in power corresponds to the point at which the flow over elements along the blade starts to separate . Field measurements of performance show that the measured output closely follows prediction at low wind speeds. As the wind speed increases, the power increases beyond the predicted peak. Rather than dropping off rapidly, the power continues to rise slowly or remains constant as the wind speed increases further. Also, there is a corresponding uncertainty in predicting dynamic blade loads in high winds, which has resulted in gross underpredictions. Except for gravitational and inertial loads, all forces acting on the blade are a result of surface pressures and, to a minor extent, viscous forces acting on the blade surface.

Several explanations have been proposed to account for the inability of current codes to predict high-wind performance. One possibility is that blade airfoil section properties are different in a steady-state, rotating flow field than in a rectilinear one. H. Himmelskamp (ref. 2) discovered through the measurement of chordwise pressure distributions that the measured lift coefficients are higher in a rotating field than one would expect from wind tunnel measurements. Not only is stall delayed to much higher angles of attack, but stall is also gentler. (His pressure distributions were measured at five radial stations on a ducted propeller.) Himmelskamp postulated that the spanwise secondary flow along the blade surface inside the separated region was somehow responsible for the increased lift. Spanwise flow of this type has been observed in the separated region on the blades of the NASA/DOE 100-kW

Mod-0 wind turbine (ref. 3). The addition of energy to the boundary layer through the use of vortex generators results in increased lift and a delay in stall on aircraft wings. It is possible that the spanwise flow on the wind turbine blade supplies this additional energy to the boundary layer, thereby delaying stall and increasing the lift coefficients to higher values than are presently being used in the computer codes.

A second possibility involves the validity of using lift and drag coefficients that have been measured in wind tunnels under steady-state, two-dimensional flow conditions. In actuality, wind turbines operate in a constantly changing three-dimensional flow field (i.e., unsteady and nonuniform). McCroskey and his colleagues have found that the section properties of airfoils operating in unsteady, three-dimensional flows can be significantly different from those measured in steady, two-dimensional flows (ref. 4). This suggests that the difference may be a result of the constantly changing nonuniform flow field in which the wind turbines operate.

The pressure distribution around the blade chord on an operating wind turbine rotor was measured to test these explanations. Ideally, the calculated lift coefficients obtained from this data could then be compared with data used in the performance codes to determine whether the values were significantly affected by the unsteady, three-dimensional flow environment. Conceivably, the pressure distributions could also be used to obtain a forcing function required for dynamic stress analysis. Therefore, a surface-pressure measurement system was developed and installed on a Mod-2, 2500-kW, wind turbine (fig. 1). Some measurements recorded with this system were previously reported in reference 5. This report includes the data presented in reference 5, together with data for the case where vortex generators were installed on the blade surface. A discussion and comparison of the measured data to that predicted by one of the performance codes is also presented. A description of the measurement system is given in the appendix.

DESCRIPTION OF APPARATUS AND TEST

The blade surface-pressure measurement system was installed on turbine 2 in the cluster of three Mod-2 wind turbines located near Goldendale, Washington. As shown in figure 1, the Mod-2 is a two-bladed machine rated at 2500 kW, using a 91-m-diameter rotor mounted upwind on a tower 61 m high. The turbine rotates at 17.5 rpm. In high winds, power is controlled with pitchable tip sections, each 13.7 m long. Except where noted, all surface pressure measurements were made in winds in which negligible tip movement occurred.

The pressure distributions were measured by means of pressure taps contained in a belt around the fixed portion of the blade at a radius of 30 m, as shown schematically in figures 2 and 3. At this station the chord length is approximately 2.4 m, and the airfoil approximates a NACA 23024 shape. Twenty-nine static surface pressures were measured around the blade chord. These pressures were fed to electronically scanned pressure sensors through 2.5- to 5-m-long tubes with an internal diameter of 1.3 mm. The tube length was dictated by the physical constraints of the installation.

Data acquisition was initiated when appropriate wind conditions were observed. Upon command, the output of the 29 sensors was scanned and

digitized at a rate of 4500 sensors per second, taking 6.4 msec to measure a set of 29 pressures. During this time, the blade moved 0.67° or 0.35 m in the tangential direction at the 30-m span location. The data sets (each consisting of 29 pressures) were transmitted to a microprocessor at a rate of 9 sets per second. The scanning and digitizing cycle was repeated until 256 data sets were in memory. The microprocessor then formatted and downloaded the data to a tape recorder for storage. The process was then repeated on command for additional wind conditions. Reduction of data from the data tapes was accomplished at the NASA Lewis Research Center.

The required fidelity of the pressure measurements depends on whether one is looking for repetitive (revolution to revolution) or nonrepetitive pressure fluctuations. For nonrepetitive fluctuations, the frequency response of the tube/sensor combination is the limiting factor. This response depends on the length and internal diameter of the tubes connecting the static pressure taps to the sensors. Tests indicated that the tube/sensor system responds to a step change in pressure somewhat like a first-order dynamic system with a time constant of less than 50 msec. This corresponds to a corner frequency of 40 Hz, which becomes the upper limit on frequency response for nonrepetitive pressure fluctuations. For repetitive fluctuations, the data set sampling rate is the limiting factor. Thirty-one sets of pressures are recorded during each revolution. Based on a conservative requirement of at least 10 samples to reasonably reproduce the highest frequency measured wave forms, the upper limit on frequency response is estimated to be about 1 Hz for repetitive fluctuations.

Together with these frequency response limits, the digitizing rate of the analog-to-digital converter introduces a time skew in each set of pressures, which affects the system fidelity. The time skew amounts to 6.4 msec between the first and the last pressure digitized in a given data set. The effect of time skew on measurement system fidelity is considered small compared to frequency response limits.

DATA ANALYSIS AND PROCESSING METHODOLOGY

Theoretically, the lift and pressure drag coefficients can be analytically determined from pressure distribution measurements in conjunction with an angle of attack (AOA) measurement. (Skin drag cannot be determined from pressure measurements.) However, it is extremely difficult to make an accurate measurement of AOA because of the variable wind conditions and the need to measure an AOA simultaneously with each data set. The AOA would have to be measured with a probe mounted on the leading edge of the blade and located in the free stream ahead of the blade. No probe was available to measure AOA, and it appeared that development of a probe with the required accuracy could not be accomplished in time for this test program. As an alternate procedure to comparing lift coefficients directly with wind tunnel measured coefficients, it was decided to plot surface pressure coefficients as a function of chord position. The shape of the plotted curves would then be compared with the shape of wind tunnel pressure distributions at angles of attack predicted by performance codes. Significant differences in the curve shapes would be an indication that the pressure distributions around the blade were being affected by the rotational, unsteady flow environment. Rotor output power would be used as the common parameter in these comparisons. This procedure is described in more detail in the subsection Comparison of Measured and Predicted C_p Curves.

The pressure coefficient is defined in terms of the dynamic pressure, the total free-stream pressure, and the static pressure as follows:

$$C_p = 1 - [(P_t - P_s)/Q] \tag{1}$$

and

$$Q = \frac{\rho}{2}(V^2 + r^2\Omega^2) \tag{2}$$

in which

C_p pressure coefficient
P_t total free-stream pressure, N/m^2
P_s static pressure, N/m^2
Q dynamic pressure, N/m^2
ρ air density, kg/m^3
V wind speed at rotor plane, m/sec
r radial distance to measurement station, 30 m
Ω rotor speed, 1.83 rad/sec

Because the wind speed at the rotor plane was small in comparison with the blade tangential speed $r\Omega$, it was neglected in the calculation of Q. The error in Q caused by neglecting the wind speed is less than 4 percent for wind speeds less than 10 m/sec, which covers most of the data presented in this report. The mean air density during the tests was 1.04 kg/m^3. With these parameters, equation (2) gives a value for Q of 1560 N/m^2 (32.5 lb/ft^2), which was used in all calculations reported herein.

As an alternative to the lift coefficient, suction and flap coefficients are useful in describing the aerodynamic forces acting on the blade. The suction coefficient C_s is defined as the normalized component of total pressure force acting in the direction of the airfoil chord. The direction of C_s is parallel to the chord in the plane of rotation for a blade with a 0° pitch angle. The flap coefficient C_f is defined as the normalized component of the pressure force acting perpendicular to the chord. Based on the coordinate system shown in figure 4, C_s and C_f are calculated from the following equations:

$$C_s = \frac{1}{2Q}\sum P_i(Y_{i+1} - Y_{i-1}) \qquad i = 1,\ldots,29 \tag{3}$$

$$C_f = \frac{1}{2Q}\sum P_i(X_{i+1} - X_{i-1}) \qquad i = 1,\ldots,29 \tag{4}$$

in which

P static pressure, N/m^2

X,Y normalized blade coordinates (fractions of chord)

i index of pressure taps

RESULTS AND DISCUSSION

Typical plots of C_p measured during wind turbine operation are shown in figure 5. This data set was recorded when the blade was passing through the horizontal position, while the machine was generating 470 kW. Figure 5(a) shows C_p as a function of the chordwise coordinate X. The upper curve is data taken on the downwind side (low pressure or suction side) of the blade. The area between the curves is proportional to C_f. A value of C_p equal to 1.0 occurs at a stagnation point on the airfoil, where the air velocity just outside the boundary layer is zero. A zero value for C_p indicates that the velocity outside the boundary is equal to free-stream velocity. Values of C_p less than zero occur in regions where the velocity outside the boundary layer is greater than the free-stream velocity. Figure 5(b) shows the same C_p data plotted as a function of the flapwise coordinate Y. The dashed line shows the data taken on the blade surface that faces the direction of rotation. The difference between the areas (1) and (2) is proportional to C_s.

Surface pressures were measured during operation with and without vortex generators (VG's) installed on the blade. Vortex generators are small tabs projecting normal to the downwind surface of the blade near the leading edge, as shown in figure 6. The purpose of these tabs is to energize the low-pressure boundary layer. This delays separation of flow and permits operation of the airfoil at higher angles of attack before separation occurs. The locations of the VG's and their measured effects on performance and blade loads are given in reference 6.

Some unpublished wind tunnel data (from the Boeing Aerospace Corporation) showing the effects of VG's on the C_p curves for a NACA 23024 airfoil are shown in figure 7. The increase in peak C_p values associated with the addition of the VG's to this airfoil is very apparent when figures 7(a) and (b) are compared. The peak C_p value with VG's is almost twice the value without VG's. The addition of VG's allows this airfoil to operate at much higher AOA before separation occurs. Thick airfoils such as NACA 23024 tend to separate quickly over a large percentage of the blade chord for a small change in AOA. Figure 7(a) shows no separation at an AOA of 12.4°, and separation at an AOA of 14.4°. Indicated by the flat portion of the upper C_p curve, separation is shown occurring in the 14.4° AOA curve starting at the 40 percent chord position. With VG's, however, the AOA is greater than 20° before separation is noticeable, as shown in figure 7(b). These figures are referred to later in this report in the subsection Comparison of Measured and Predicted C_p Curves.

Pressure coefficients measured on the rotating blade with and without VG's, together with calculated values of C_s and C_f, are shown in figures 8 to 10. The data acquisition was initiated when strip chart recordings of wind velocity and machine output power indicated that wind conditions were reasonably stable. Data sets for three consecutive revolutions are shown in each figure to give an indication of the amount of variation occurring from revolution to revolution. The values of C_p are plotted as a function of chord position with the downwind side (low pressure or suction side) shown on the left. (For clarity, symbols indicating data points are not plotted.) The leading edge of the airfoil is to the left, where the percent chord location equals zero. The C_p scale is located between the curves. A scale of rotor position is on the right, in which a rotor position of 0° indicates that

the instrumented blade is at the 6 o'clock position. Time increases vertically.

Changes in the spacing between the C_p curves indicate changes in the curve shapes. Areas where the curves are more closely spaced indicate decreasing values of C_p. Conversely, areas where the spacing between the curves becomes larger indicate increases in the C_p values. Calculated values of C_s and C_f for each curve are shown on the right side of the figure. The vertical position of the C_s and C_f values gives the rotor position at which the pressures were measured, and can be used to locate the zero value for the C_p scale for individual curves. A positive value of C_s produces torque in the direction of rotation and positive output power. A positive value of C_f produces a force perpendicular to the plane of rotation and in the direction of the tower. Average values of C_s and C_f for the three revolutions are indicated in each figure. (Note: For 1 m of span length at the measurement station, a C_s value of 0.1 produces 21 kW, while a C_f value of 1.0 produces 3.8 kN of force bending the blade toward the tower.)

Measurements on Blade Without Vortex Generators

Plots of chordwise pressure coefficients for the case when the blades were operating without VG's are shown in figure 8. The following important observations can be made:

(1) At low wind speeds (i.e., low output power levels), the flow remains fully attached, as shown in figures 8(a) and (b).

(2) Figures 8(c) and (d) present pressure data at a medium wind speed, in which the flow separates for a brief period and then quickly reattaches. The separation occurs at a rotor position of about 225°.

(3) As the wind speed increases further, separation occurs over more of a revolution, until the flow is fully separated over an entire revolution, as shown in figure 8(e).

(4) Unsteady flow effects are indicated by local ripples that come and go in the C_p curves at all wind speeds as the blade rotates.

(5) The changes in spacing between the curves and the variation in C_s and C_f values reflect the nonuniform spatial distribution of the wind velocity and/or direction.

Figure 8(a) shows a set of data taken when the machine was producing 470 kW. The cyclic variation in C_s shown in the figure was a result of the rotor plane not being aligned perpendicular to the wind. Values of C_s are generally negative, indicating that the airfoil at this measurement station actually retards the rotation of the blade. One could conclude that, at larger radii, C_s would also be negative, and therefore all output power was being produced by the inner portion of the blade. Note that no separation occurred, and that cyclic changes in C_s and some ripples in the C_p curves were probably caused by wind velocity gradients and turbulence.

Figure 8(b) shows data taken when the machine was producing 870 kW. The C_p distributions are well behaved, with a small amount of cyclic variation. The C_s coefficients are all positive, indicating the production of positive torque at this blade station. During a revolution, C_s is maximum when the blade is in the top (180°) position. This would be expected, since the wind velocity tends to increase as a function of height above ground because of wind shear. The machine appears to be aligned with the wind because the peak and minimum values of C_s occur at approximately the 0° and 180° rotor positions. The average value of C_s for three revolutions is 0.069 compared with a value of -0.011 for the 470-kW-power case in figure 8(a).

For figure 8(c), the output power was 1500 kW. This figure shows the flow separating at about the 225° location, with quick jumps from attached flow to separated flow and back to attached flow over a 30° to 40° interval of rotation. The separation is shown to cause a definite dropoff in the C_s values. The cyclic variation in C_s is apparent, with the peak and minimum values occurring at the same rotor positions as shown in figure 8(b). The average value of C_s has risen to 0.109 even though separation appears during each revolution.

Figure 8(d) shows data taken when the output power was 2210 kW. The flow is separated over a greater portion of each revolution, with C_s showing a larger variation in values. The separation occurs when the rotor is at the top (180°) position, and small but discernable changes in C_s are shown as the rotor passes in front of the tower. The average C_s has reached a value of 0.118, which was the highest average value measured for the blade without VG's. Individual values are approaching 0.2, which is significantly larger than the peak value of 0.149 for the wind tunnel data shown in figure 7(a).

The output power is 2470 kW for the data shown in figure 8(e). In this figure, the flow appears to be separated over almost all of each revolution. As the rotor approaches the 0° position, the flow apparently attaches briefly, with a corresponding increase in C_s. Here, large variations in C_s result in large fluctuations in rotor torque generated at this blade station. The average C_s has dropped to 0.046, which indicates that most of the power is being generated by the tip section. One would expect that if C_s is 0.046 at this station, it would be less at smaller radii and would probably take on negative values near the hub. Even with separation occurring over most of the revolution, the value of C_s indicates the production of positive torque at this blade station.

Measurements on Blade With Vortex Generators

In figure 9 are plots of surface pressure coefficients for the case when VG's were installed on the blade. It should be noted that the wind velocity required to produce a given output power level is about 10 percent lower when VG's are installed on the blade, and therefore it is felt that comparison of C_s coefficients with and without vortex generators is not meaningful. The following general observations can be made:

(1) The most significant observation is that the VG's prevented flow separation at the 30-m radius for power levels up to 2570 kW.

(2) The C_s values changed in a somewhat cyclic manner with very little random fluctuations.

(3) As with the results shown in figure 8, the local variations in the pressure coefficient curves were probably the results of small-scale turbulent fluctuations in the wind. The cyclic variation in C_s was a result of variation in the wind velocity with height.

The output power was 440 kW for the data shown in figure 9(a). The values of C_s show minimal cyclic variation with rotor position and average 0.04 for the three revolutions.

Figure 9(b) shows data taken when the machine was producing 1490 kW. The average value of C_s is 0.103. No separation appears in this figure, whereas figure 8(c) shows the start of separation for a similar power level without VG's.

The data in figure 9(c) was recorded at a power output of 2470 kW. The average C_s value is 0.154, which is more than three times the value for the data shown in figure 8(e) for approximately the same power level without VG's. Some dropoff in C_s is seen as the blade passes the tower. At the top (180°) position, C_s reaches a peak value.

Data are shown in figure 9(d) for the case when the power output was 2570 kW. The average C_s has reached 0.18, and the C_p curves show no signs of separation. At this point, the blade tips were beginning to move to control power, and this resulted in an increased discontinuity in the blade surface and a gap less than one chord length outboard of the pressure sensors. However, the VG's appear to be able to maintain attached flow in spite of the nearby discontinuity.

A final set of data is shown in figures 10(a) and (b), again for the case with VG's installed. The output power for these figures was 2680 kW, with the tip section actively controlling machine power. The average C_s in figure 10(a) is 0.27, which is more than 2.3 times the maximum value calculated for any of the pressure data measured without VG's. Some separation is shown to occur in figure 10(b). This was the only revolution in the data set in which separation occurred. Here again, this figure shows how quickly the flow separates and then reattaches. It also shows the sharp dropoff in C_s, which is a result of separation, changing from 0.3 to -0.05 while the rotor moves about 35°. This would be expected to introduce a large change in torque force at this radius, and a corresponding change in output power. However, the change in output power would not necessarily be as abrupt as might be inferred from this figure because of the integration of torque forces from tip to tip of the rotor.

Comparison of Measured and Predicted C_p Curves

Plots were made to see if any differences in shape of the C_p curves were apparent for C_p's measured on the wind turbine and for those measured in wind tunnel tests. A set of typical C_p curves measured at various conditions of output power and wind velocity are shown in figure 11. These curves were taken from the data sets shown in figures 8 and 9, with and without VG's, when the

blade was passing through the 270° (horizontal, descending) position. A comparison of the curves in figures 11(a) and (b) with those in figures 7(a) and (b) reveals that the peak C_p magnitudes measured on the wind turbine are significantly higher than any of those measured in the wind tunnel.

For the case without VG's, shown in figures 7(a) and 11(a), the peak magnitude of C_p has increased from 3 to 4. This increase in peak magnitude suggests that the airfoil sections are operating unstalled at higher angles of attack than would be expected from wind tunnel data. This implies that separation may be delayed as a result of the rotational flow field. As suggested in the Introduction, the effect of rotation could be considered to be similar to the effect of VG's, that is, to delay separation and increase the peak value of C_p.

Comparison of figures 8(b) and 11(b), without and with VG's, respectively, shows an increase in peak values measured on the wind turbine, but one of smaller magnitude. Here, too, the rotating flow field appears to delay separation when VG's are installed on a rotating blade.

A second set of plots was made to determine how the wind turbine C_p distributions compared with wind tunnel C_p distributions at various rotor powers. This was accomplished by first calculating the AOA at the 30-m span position as a function of rotor power, using the WIND-2 performance code. The AOA values thus found were used to choose the appropriate wind tunnel C_p curves from figure 7, which theoretically produced the same rotor power for which measured C_p data were available. Comparison plots for the data sets shown in figures 8 and 9 are shown in figures 12 and 13, which include calculated values of AOA and rotor power.

For each of the power levels shown in figures 12 and 13, the curves for the measured wind turbine data are higher than the curves derived from wind tunnel data. The fact that the turbine C_p coefficients are higher for a given rotor power than those predicted by using the performance code and wind tunnel data implies that the wind velocity to produce the power is lower. Therefore, the test performance is better than predicted.

In summary, it is concluded that the three-dimensional flow field associated with a rotating wind turbine blade, by some mechanism as yet undefined, causes a change in the surface pressure distribution around the blade. This results in higher values of C_s than would be predicted from performance codes that use two-dimensional lift and drag data measured in a wind tunnel.

CONCLUDING REMARKS

A set of data has been presented showing the chordwise distribution of pressure coefficients measured on an operating Mod-2 wind turbine. Data were presented for blades with and without vortex generators (VG's) mounted on the downwind surface. As expected, the vortex generators were shown to change the shape of the pressure coefficient curves by significantly increasing the peak values and delaying separation.

The data sets showed the flow rapidly separating and reattaching to the blade surface. The amount of time during each revolution that the flow was separated depended on the wind velocity gradient. The variation of suction and flap coefficients resulting from the flow separation was vividly illustrated. This rapidly changing suction coefficient would be expected to produce rapid changes in rotor torque and power output. Similarly, the large changes in flap coefficient would be expected to produce fluctuations in the blade bending moments and corresponding cyclic changes in blade stress levels.

A comparison of the measured pressure coefficient curves with those obtained from wind tunnels indicated that the magnitude of peak values measured on the wind turbine were significantly higher. This was true for both cases, with and without vortex generators. This implies that separation is being delayed because of the three-dimensional flow field associated with the rotating blade. The measured pressure coefficient distributions were also compared with those obtained from wind tunnel tests for equal power levels. This comparison showed that, at all power levels for which data were available, peak magnitudes of the measured pressure coefficients were higher than those which would be predicted from current performance codes and wind tunnel airfoil data. This suggests that the three-dimensional flow field is changing the pressure distribution on the blade surface. This results in higher values of suction coefficient, and therefore more rotor power for a given wind condition than would be predicted.

APPENDIX - DESCRIPTION OF MEASUREMENT SYSTEM

The blade chord pressure measurement system was originally designed for and installed on the DOE/NASA 100-kW Mod-0 wind turbine located near Sandusky, Ohio. The system was modified to meet the installation constraints of the Mod-2 wind turbine. Figures 2 and 3 show schematic diagrams of the location of the system components on the Mod-2. In the following sections, a description of the pneumatic system is followed by a description of the data acquisition and control system. The pneumatic system includes the pressure belt, pressure transmission lines, purge valve, a 32-channel pressure sensor, and a pneumatic control module. The data acquisition and control system consists of a sensor control module, a decode module, and a microprocessor.

Pneumatic System

The pressures developed around the blade chord were sampled with a set of 29 static pressure taps. The taps were 1.0 mm in diameter and were bored into tubes with a tool similar to a cork borer. Ten tubes, 1.3-mm i.d. and 3.2-mm o.d., were molded together to form a ribbon. The pressure belt was made up of four ribbons, as shown in figure 14. The tubing downstream of a pressure tap was plugged with rubber sealant so that the pressure tap was effectively located at the end of a pressure transmission line. This plug also allowed a given tube in a ribbon to be used for two pressure taps, one on either side of the blade.

Twenty-nine static pressure taps were bored in the belt starting where the chord line intersects the leading edge and at 2.5, 5, 7.5, 10, 15, 20, 25, 30, 40, 50, 60, 70, 80, and 90 percent chord stations on both the upwind (high pressure) and downwind (low pressure) sides of the blade. Two inner ribbons in the belt contained the static taps, while the two outer ribbons were used to even out the flow over the belt. The ribbons were cemented to the blade with rubber sealant starting and ending at the trailing edge. The pressure transmission tubes were taped to the trailing edge and led over the downwind side of the blade and through the "D" hatch. Figure 3 shows a diagram of the tubing layout. The "D" hatch is built into the blade to allow access to the pitch control components for maintainance purposes. Short lengths of stainless steel tubing were formed into elbows and used to make the turns at the trailing edge.

The response of the pressure tap connecting tubing and transducer to varying pressure was determined by applying a step pressure change to a similar configuration and by recording the transducer output as a function of time. Tube lengths in this installation varied between 2.5 and 5 m. A typical response curve is shown in figure 15. For a 2.5-m-long transmission tube, the response appears to be overdamped and can be considered as having a time constant of 0.025 sec. This corresponds to a 6.3 Hz corner frequency, at which the output amplitude for an input sine wave would be reduced by 3 dB (70 percent). The data system sampled the pressures every 11° of rotor rotation so that no high-frequency fluctuations of pressure were seen directly in the recorded data.

A total pressure was also recorded as part of the data and was measured with a shielded probe mounted on the upwind side at the 25 percent chord location. This probe was shown by calibration to be insensitive to changes in

flow direction within ±45° of its nominal installation direction. The relative position of this probe is shown in figure 3. Two "constant" pressures generated in a sealed volume were also fed to the pressure sensor for a total of 32 pressures measured by the system. Monitoring of the two constant pressures was used to verify system operation.

A schematic diagram of the pneumatic connections between the purge valve and the pressure sensor components mounted on the "D" hatch is shown in figure 16. A diagram of the internal valving for one of the 32 inlet lines in each of these two components is shown in figure 17. Operation of the slide valves was controlled by four independent pressures. As shown in figure 17(a), pressurizing control line P1 placed the purge valve slider in the normal operating position with the input port directly connected to the output port. Pressure on control line P2 switched the slider so that the inlet port could be purged with dry air to remove accumulated moisture in the tubing. At the same time, the calibration port was connected to the outlet port.

Figure 17(b) shows the valve arrangement for the pressure sensor. Pressurizing line P3 on the sensor positioned its slider so that the inlet port connected directly to the internal pressure transducer. Pressurizing line P4 connected the calibration port to the transducer. As indicated in figure 16, the calibration port on the sensor was externally connected to the reference port. Thus, when P4 was pressurized, the transducer zero could be measured while the machine was rotating. All 32 sensors had common reference and calibration ports.

The four control lines, the purge line and calibration lines from the purge valve, and the reference line from the sensor were led through the inside of the blade to the rotor hub. The static pressure in the open area of the hub was used as the reference pressure for the pressure sensor. Purge air and calibration pressures were supplied from the nacelle through temporary tube connections that were made only when the machine was shut down. A control pressure of 552 kN/m^2 (80 psi), supplied from a high-pressure gas bottle and regulator mounted in the hub, was used in this system. The control pressure was connected to the control lines through three-way valves, which were mounted in the hub and operated by the decode module described in the following section.

Data Acquisition and Control

The pressure measuring device in the system was a commercial sensor that contained 32 miniature semiconductor strain-gauge transducers. It was built with an internal electronic multiplexer that scanned the individual transducers. The output of the multiplexer was amplified to ±5 V dc, full scale. The transducers measured the pressure difference between an input pressure and a reference pressure. The transducers were ranged for 34.5 kN/m^2 (±5.00 psi) differential pressure, full scale. Each transducer was specified to have a maximum static error of 0.15 percent full scale, with a maximum thermal sensitivity and zero shift of ±0.03 percent of full scale per degree Celsius. Electrical connections to the sensor included five address lines for controlling the multiplexer, the sensor output, and the power supply lines.

The sensor control module was designed to (1) set up the addressing for the mutliplexer, (2) digitize the sensor output, (3) temporarily store the digitized data, and (4) transmit the stored data to the microprocessor on request. The module operated in two separate modes: (1) a digitizing and storage mode, and (2) a transmit mode.

A block diagram of the sensor control module configured in the digitizing and storage mode is shown in figure 18(a). Sensor output was fed into a 14-bit analog-to-digital converter (A/D), the serial output of which was stored in a 512-bit random access memory. A 4500-Hz free-running clock continuously initiated A/D conversions. Each transducer output was stored as a 16-bit word (14 bits from the A/D and 2 dummy bits). This design resulted in the continuous updating of memory with the most recent pressure measurements. At 4500 sensors per second, the sensor control module scanned the 29 pressures on the belt in 6.4 msec, during which time the blade rotated 0.67°.

The sensor control module switched to the data transmit mode after receiving a data request signal sent from the decode module. A diagram of the sensor control in the transmit mode is shown in figure 18(b). When a data request was received, the sensor control module completed the digitizing and storage cycle it was in, and then switched to the transmit mode. The clock pulses were fed to the counter, the output of which addressed the memory. The data in memory were serially transmitted together with the clock signal and a clock-divided-by-eight signal to the decode module in the hub. At a rate of 4500 Hz, it took 0.106 sec to send the 512 bits to the decode module, during which time the blade moved 11.2°. It was this transmit time that limited the rate at which data could be recorded by this measurement system. After 512 bits had been transmitted, the sensor control module switched back into the digitizing and storage mode.

A decode module located in the blade hub received the transmitted data and clock pulses from the sensor control module, converted them to RS-232 format, and sent them to the microprocessor located in the control room. The decode module received commands by way of the RS-232 line from the microprocessor and operated three-way valves that controlled pressures to the slide valves. The data request signal was also generated from the command in the decode module.

The microprocessor was programmed to generate the command signals sent to the decode module. Along with the sensor data, the microprocessor digitized machine operating conditions such as output power, wind speed, rotor position, rotor speed, atmospheric pressure, and yaw error and added these variables to the sensor data. The microprocessor had sufficient memory to store 256 sets of data, after which the data were downloaded to a digital tape recorder. The digital cassette tapes were sent to NASA Lewis, where data were reduced to engineering units and analyzed.

REFERENCES

1. Viterna, L.A.; and Janetzke, D.C.: Theoretical and Experimental Power from Large Horizontal-Axis Wind Turbines. DOE/NASA/20320-41, NASA TM-82944, 1982.

2. Himmelskamp, H.: Profiluntersuchungen an Einem Umlaufenden Propeller. Diss. Gottingen 1945. Max-Planck-Inst. fur Stromungsforschung, Gottingen Report No. 2, 1950. (Cited in Schlichting, H.: Boundary Layer Theory, 7th ed., McGraw Hill, 1979).

3. Savino, J.M.; and Nyland T.W.: Wind Turbine Flow Visualization Studies. Windpower '85, CONF-850834, 1985, pp. 559-564.

4. McCroskey, W.J.: The Phenomenon of Dynamic Stall. Unsteady Airloads and Aeroelastic Problems in Separated and Transonic Flow, VKI-LS-1981-4, Von Karman Institute for Fluid Dynamics, Belgium, 1981, pp. 2-1 to 2-28. (NASA TM-81264).

5. Nyland, T.W.: Chordwise Pressure Measurements on a Blade of the Mod-2 Wind Turbine. Proceeding of the Sixth ASME Wind Energy Symposium, ASME, 1987, pp. 33-40.

6. Sullivan, T.L.: Effect of Vortex Generators on the Power Conversion Performance and Structural Dynamic Loads of the MOD-2 Wind Turbine. NASA TM-83690, DOE/NASA/20320-59, 1984.

FIGURE 1. - DOE/NASA MOD-2 2500-kW EXPERIMENTAL WIND TURBINE LOCATED NEAR GOLDENDALE, WASHINGTON.

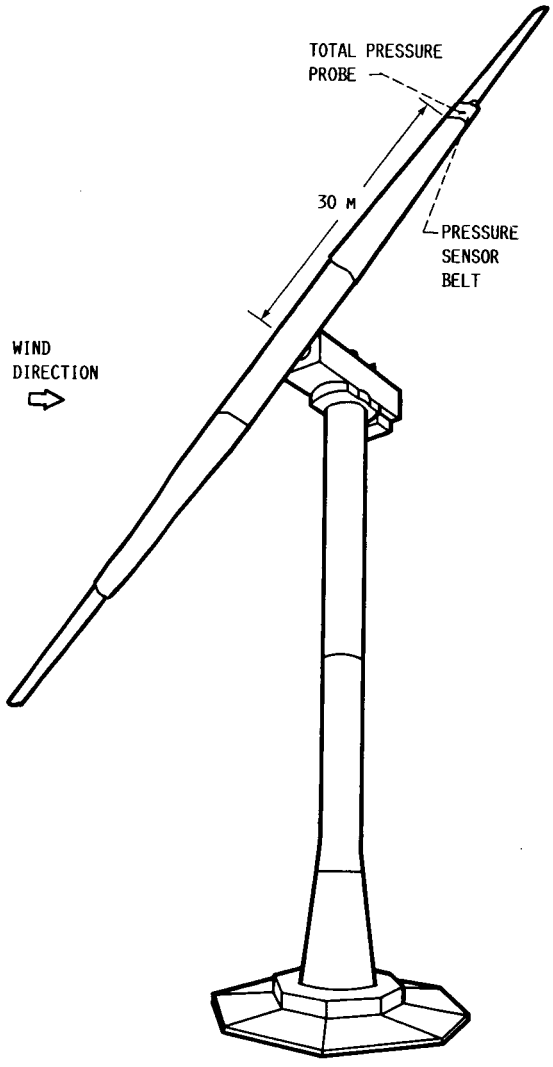

FIGURE 2. - SCHEMATIC DIAGRAM OF MOD-2 WIND TURBINE, SHOWING LOCATION OF PRESSURE SENSOR BELT AND TOTAL PRESSURE PROBE.

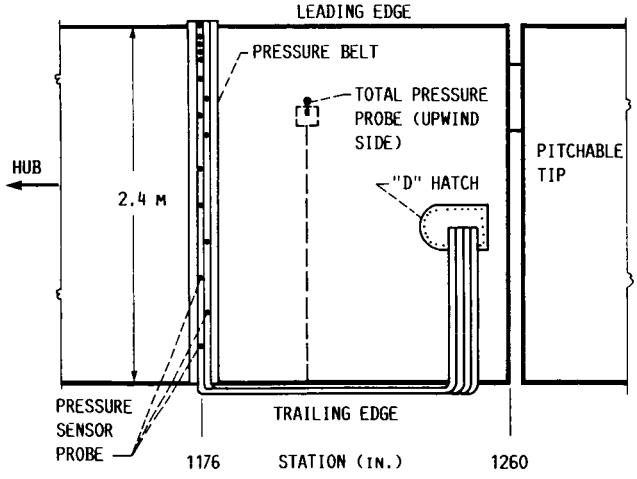

FIGURE 3. - CLOSEUP SCHEMATIC VIEW OF PRESSURE BELT INSTALLATION, SHOWING DOWNWIND SIDE WITH TUBING LEADING INTO BLADE THROUGH "D" HATCH.

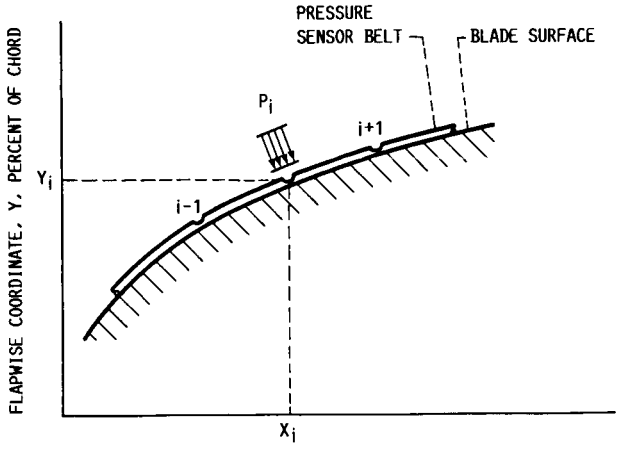

FIGURE 4. - BLADE SURFACE COORDINATE SYSTEM, WHERE P IS STATIC PRESSURE AND i IS INDEX OF PRESSURE TAPS.

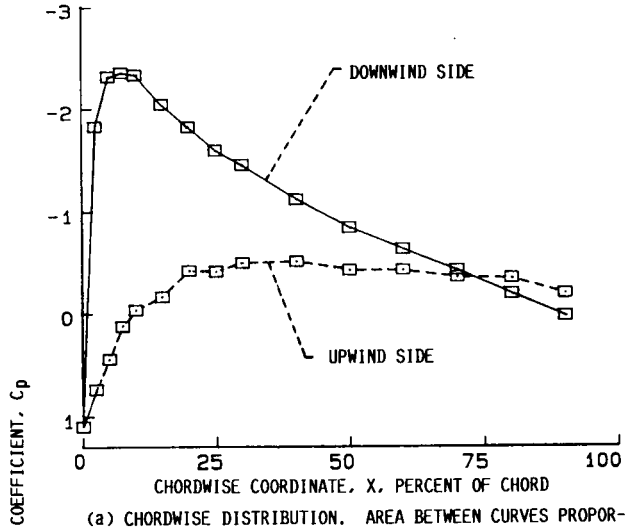

(a) CHORDWISE DISTRIBUTION. AREA BETWEEN CURVES PROPORTIONAL TO FLAP COEFFICIENT.

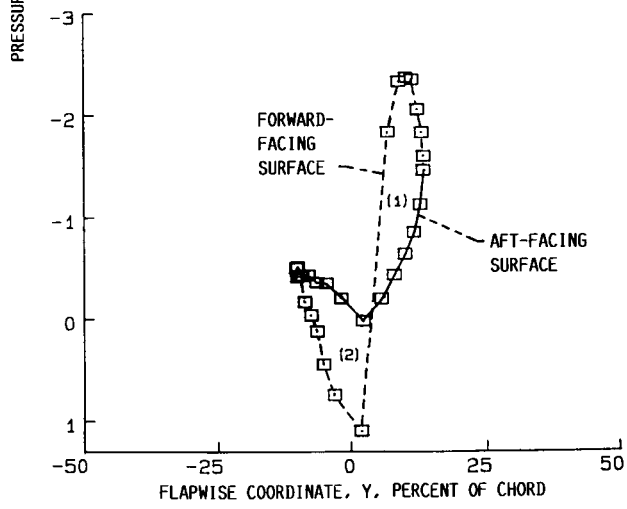

(b) FLAPWISE DISTRIBUTION. AREA (1) MINUS AREA (2) PROPORTIONAL TO SUCTION COEFFICIENT.

FIGURE 5. - TYPICAL PRESSURE COEFFICIENTS MEASURED FOR MOD-2 WIND TURBINE AT 470 kW.

ORIGINAL PAGE IS
OF POOR QUALITY

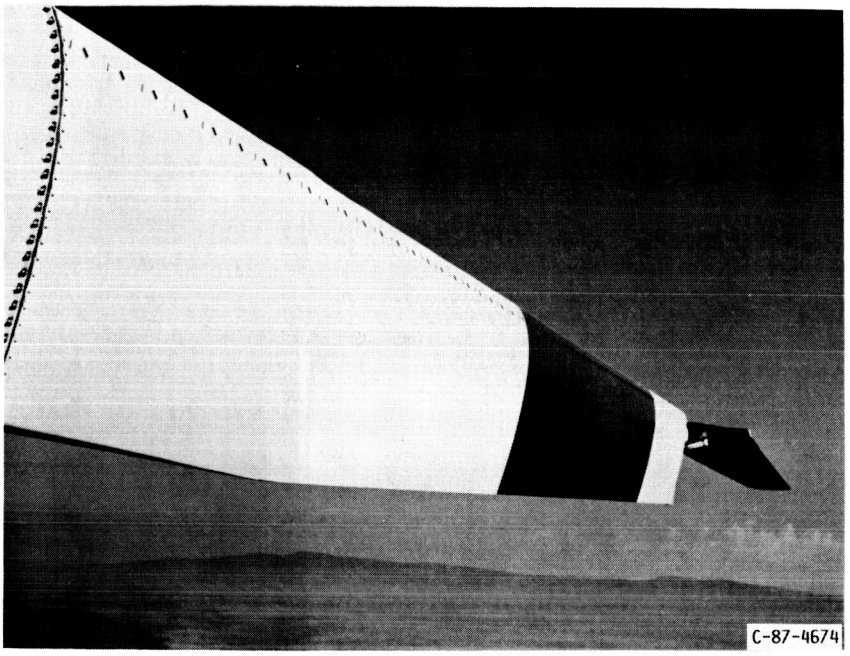

FIGURE 6. - VIEW OF LOW-PRESSURE SURFACE OF MOD-2 WIND TURBINE BLADE, SHOWING ROW OF VORTEX GENERATORS NEAR LEADING EDGE. TIP SECTION IN FEATHERED (STOPPED) POSITION.

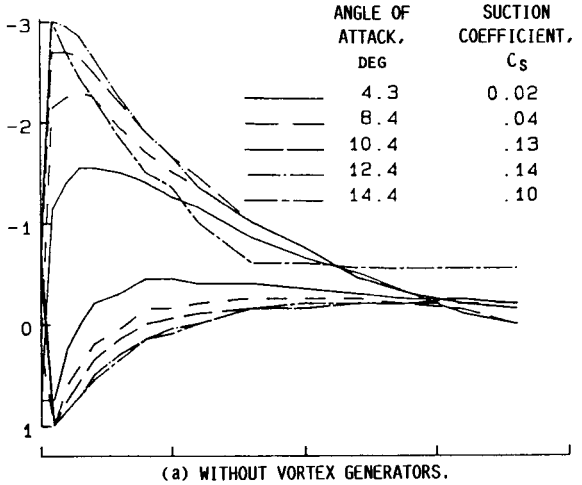

(a) WITHOUT VORTEX GENERATORS.

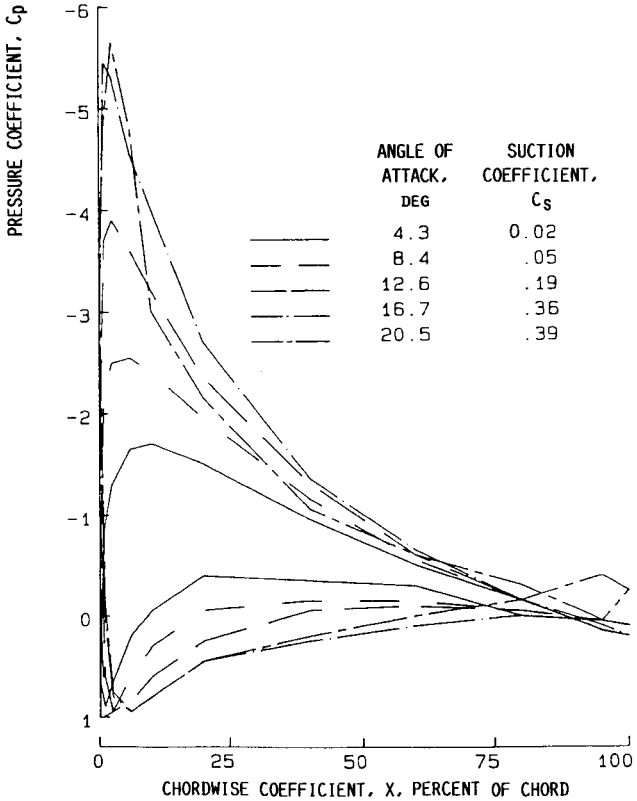

(b) WITH VORTEX GENERATORS, IN CONFIGURATION SHOWN IN FIGURE 6.

FIGURE 7. - PRESSURE COEFFICIENTS MEASURED IN WIND TUNNEL ON NACA 23024 AIRFOIL (UNPUBLISHED DATA FROM BOEING AEROSPACE CORP.).

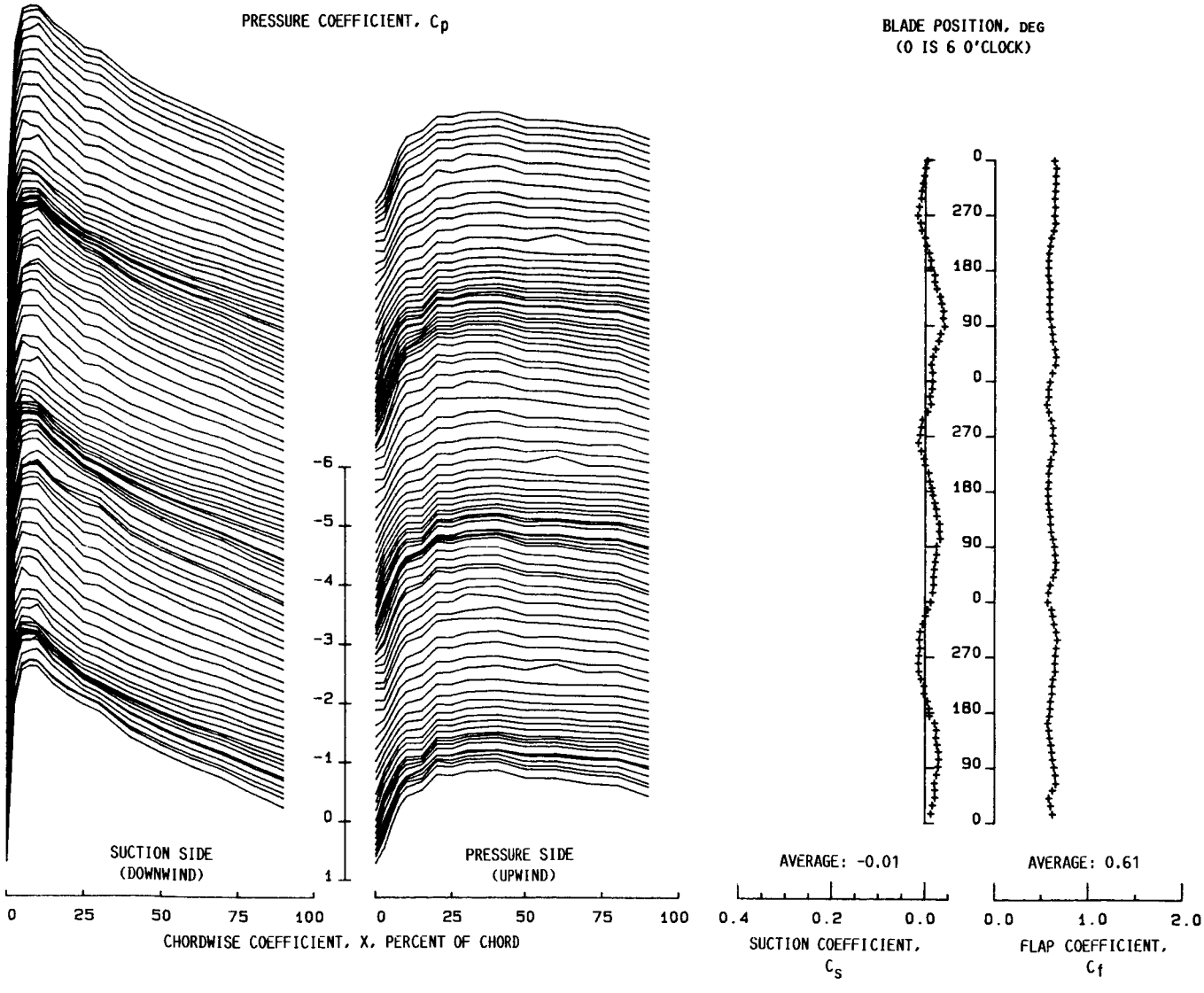

(a) 470-kW POWER OUTPUT.

FIGURE 8. - PRESSURE, SUCTION, AND FLAP COEFFICIENTS MEASURED ON MOD-2 WIND TURBINE BLADE WITHOUT VORTEX GENERATORS.

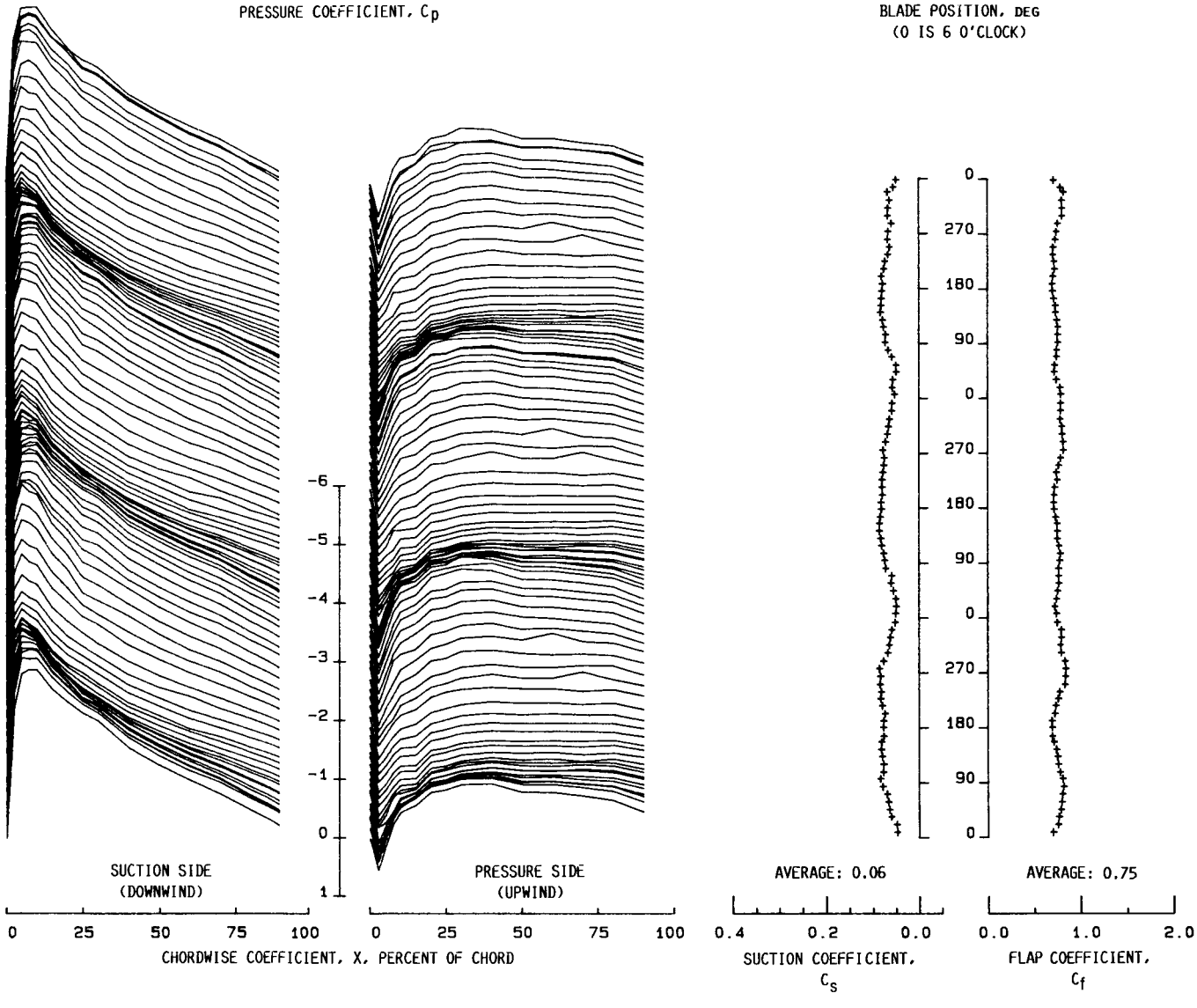

(b) 870-kW POWER OUTPUT.

FIGURE 8. - CONTINUED.

ORIGINAL PAGE IS
OF POOR QUALITY

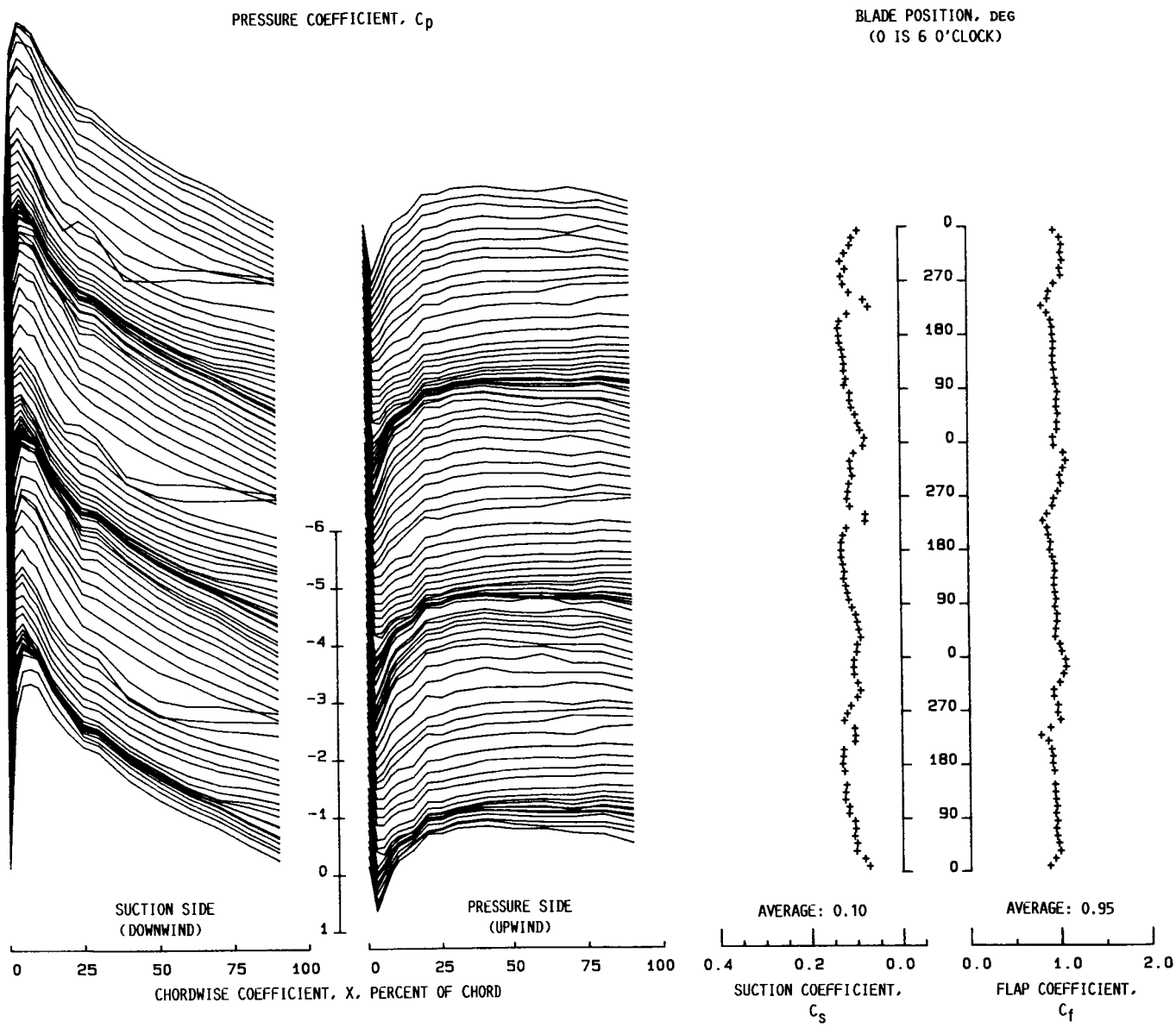

(c) 1500-kW POWER OUTPUT.

FIGURE 8. - CONTINUED.

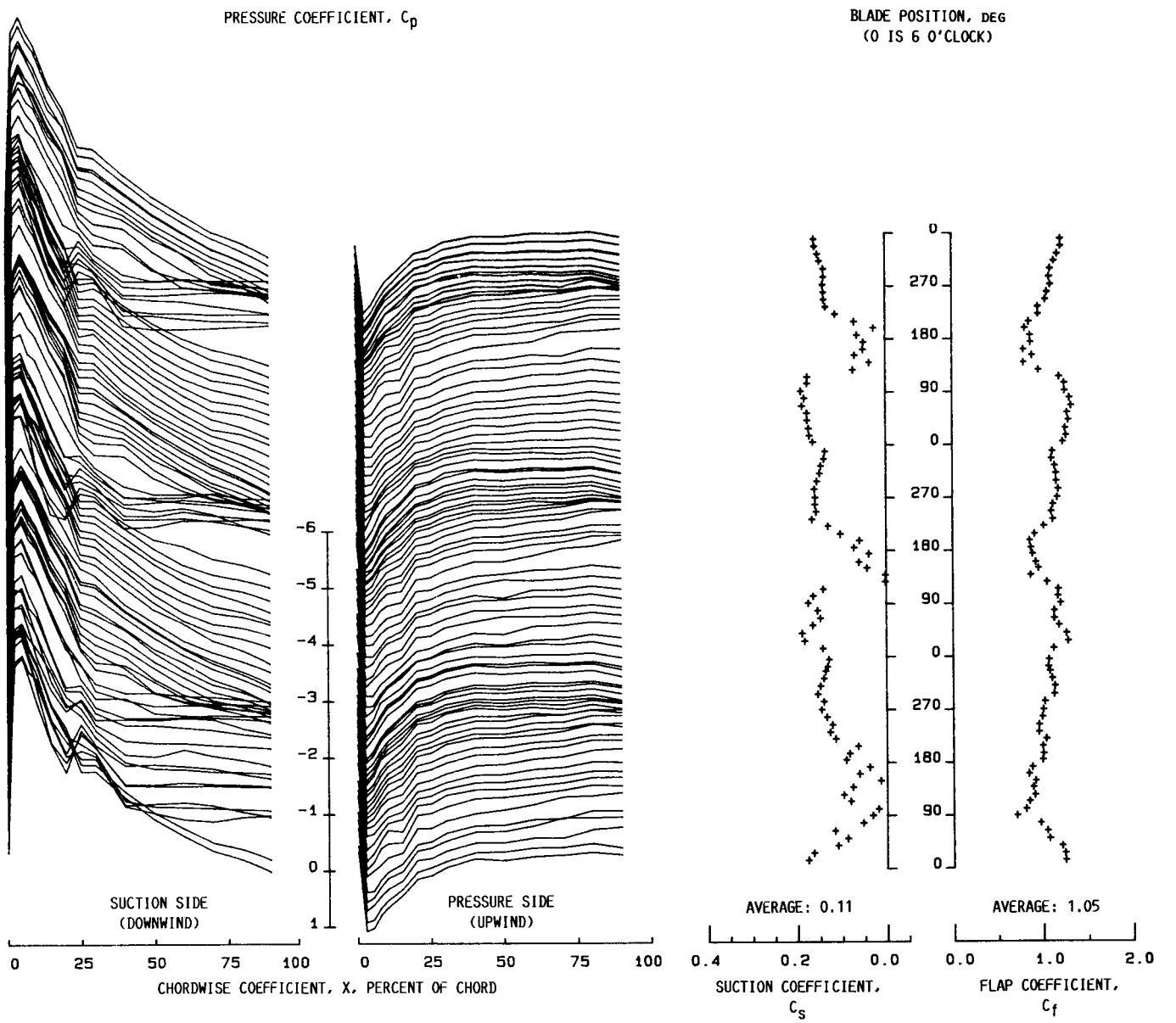

(d) 2210-kW POWER OUTPUT.

FIGURE 8. - CONTINUED.

ORIGINAL PAGE IS
OF POOR QUALITY

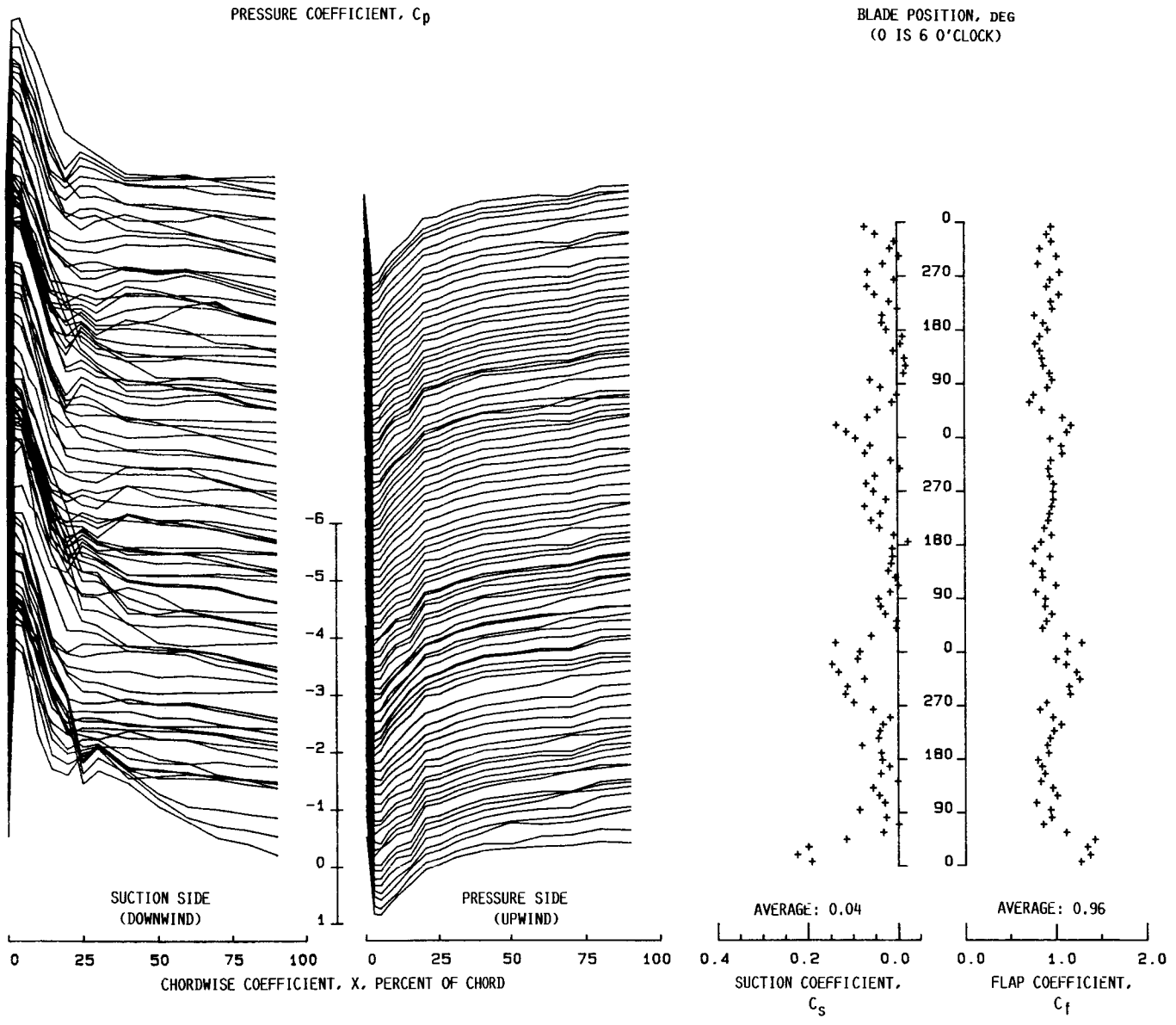

(e) 2470-kW POWER OUTPUT.

FIGURE 8. - CONCLUDED.

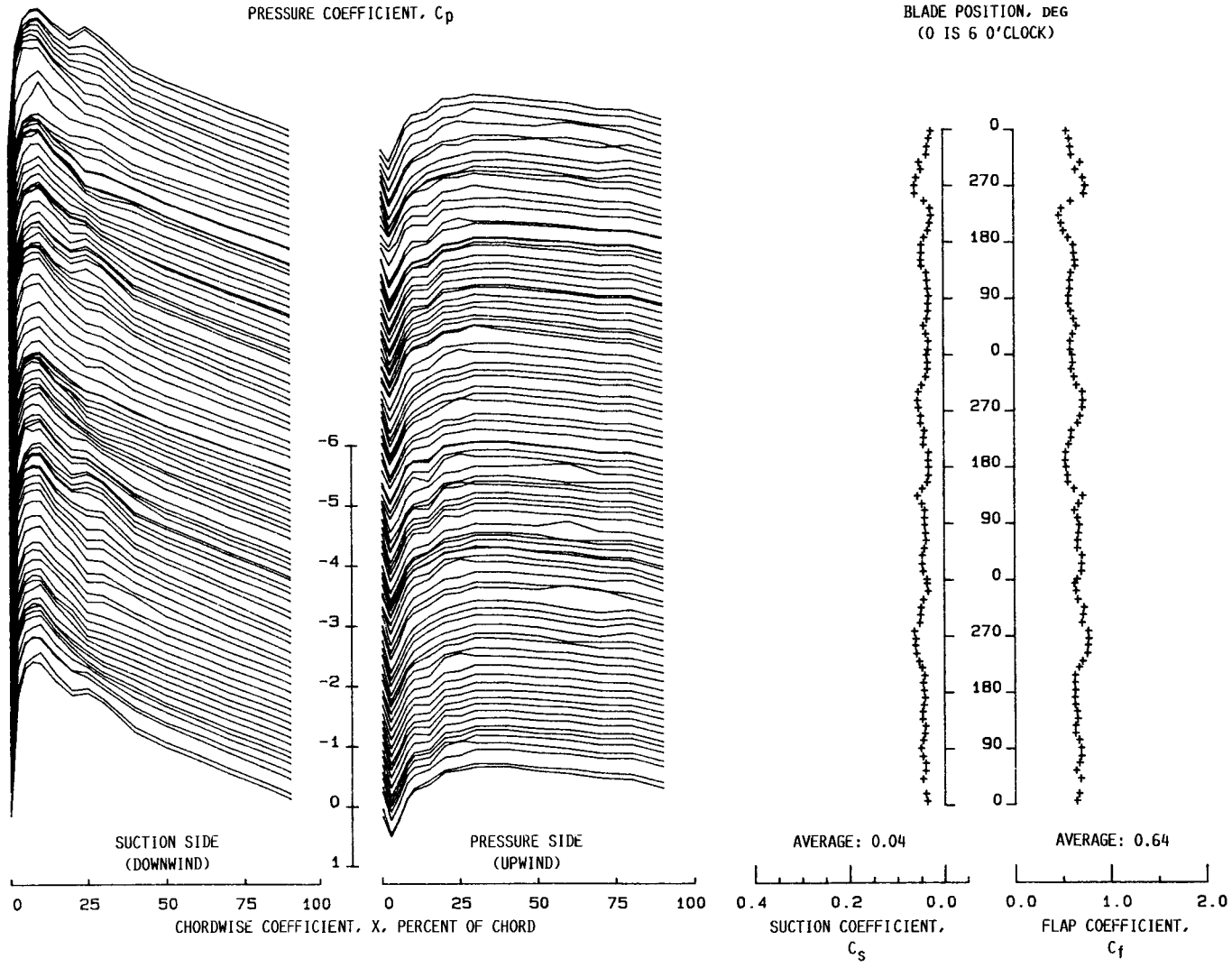

(a) 440-kW POWER OUTPUT.

FIGURE 9. - PRESSURE, SUCTION, AND FLAP COEFFICIENTS MEASURED ON MOD-2 WIND TURBINE BLADE WITH VORTEX GENERATORS INSTALLED.

ORIGINAL PAGE IS
OF POOR QUALITY

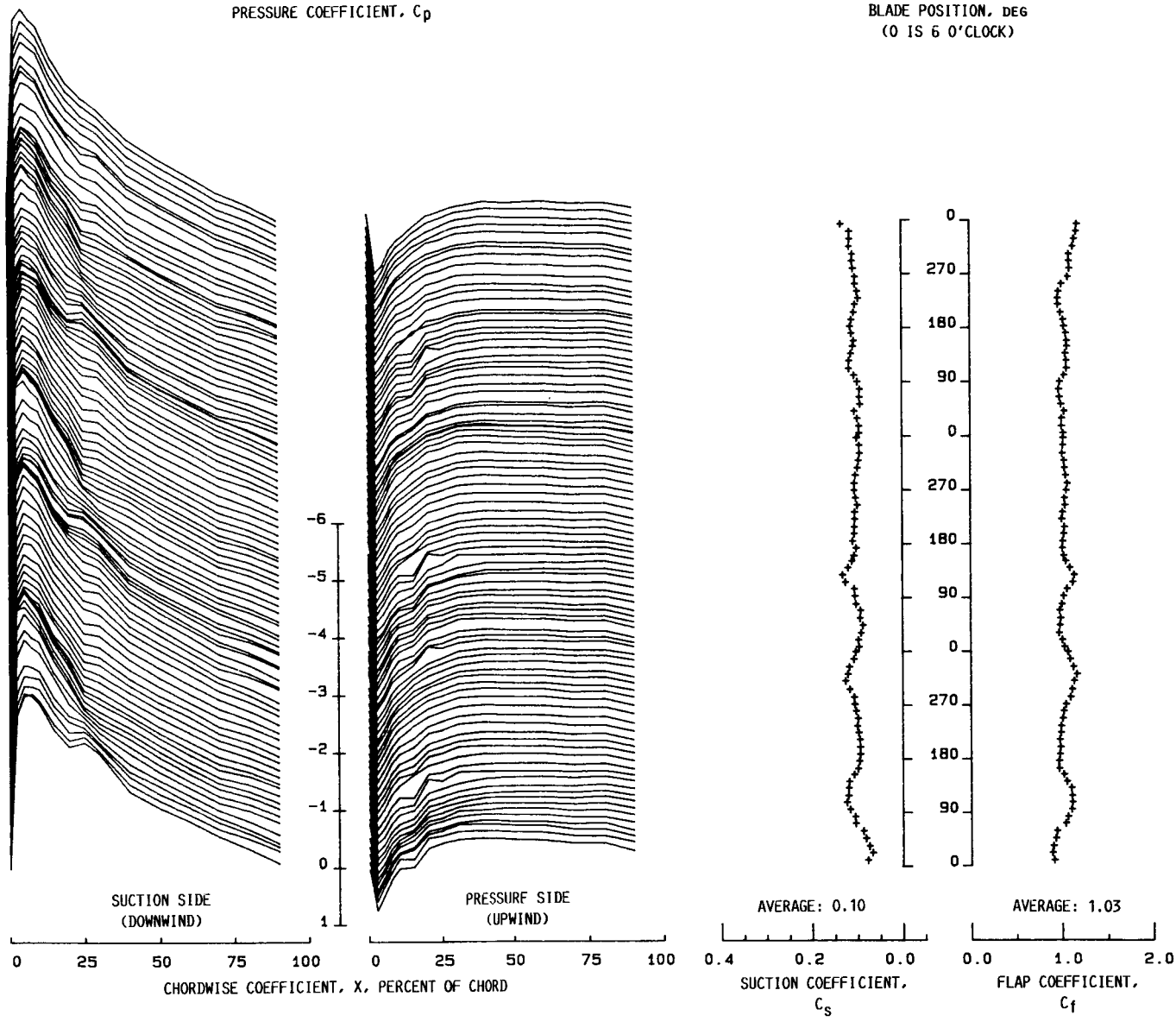

(b) 1490-kW POWER OUTPUT.

FIGURE 9. - CONTINUED.

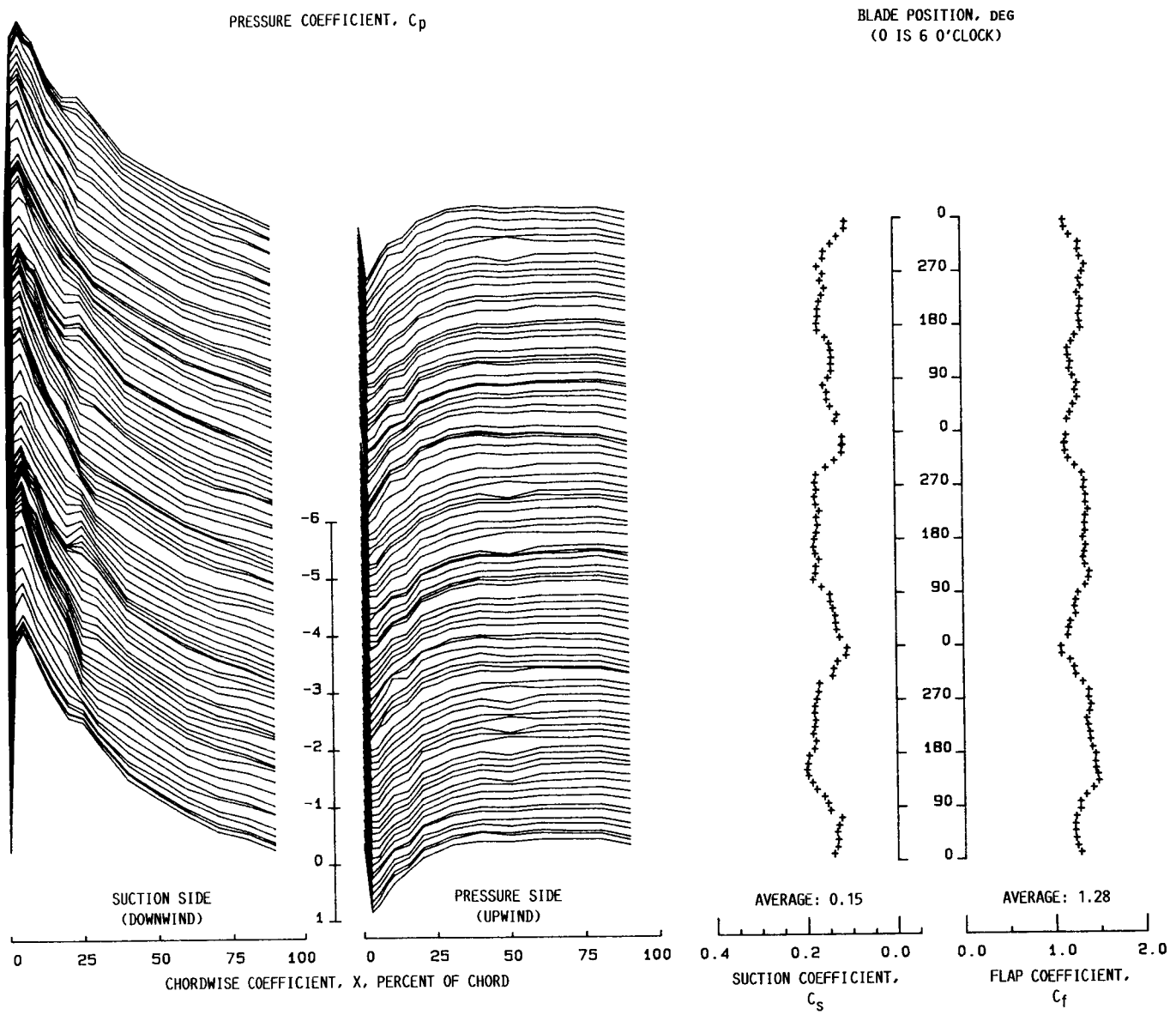

(c) 2470-kW POWER OUTPUT.

FIGURE 9. - CONTINUED.

ORIGINAL PAGE IS
OF POOR QUALITY

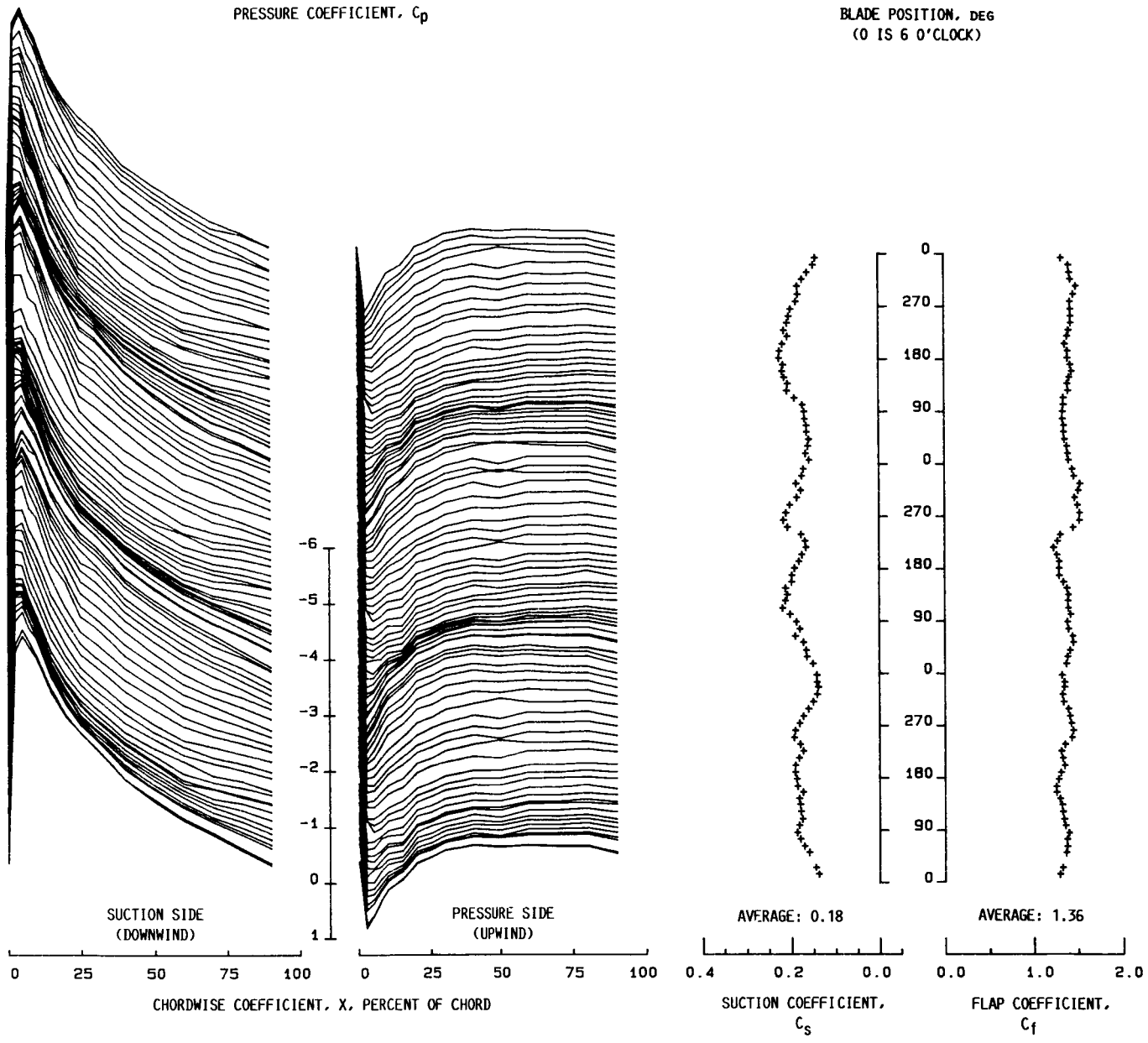

(d) 2570-kW POWER OUTPUT.

FIGURE 9. - CONCLUDED.

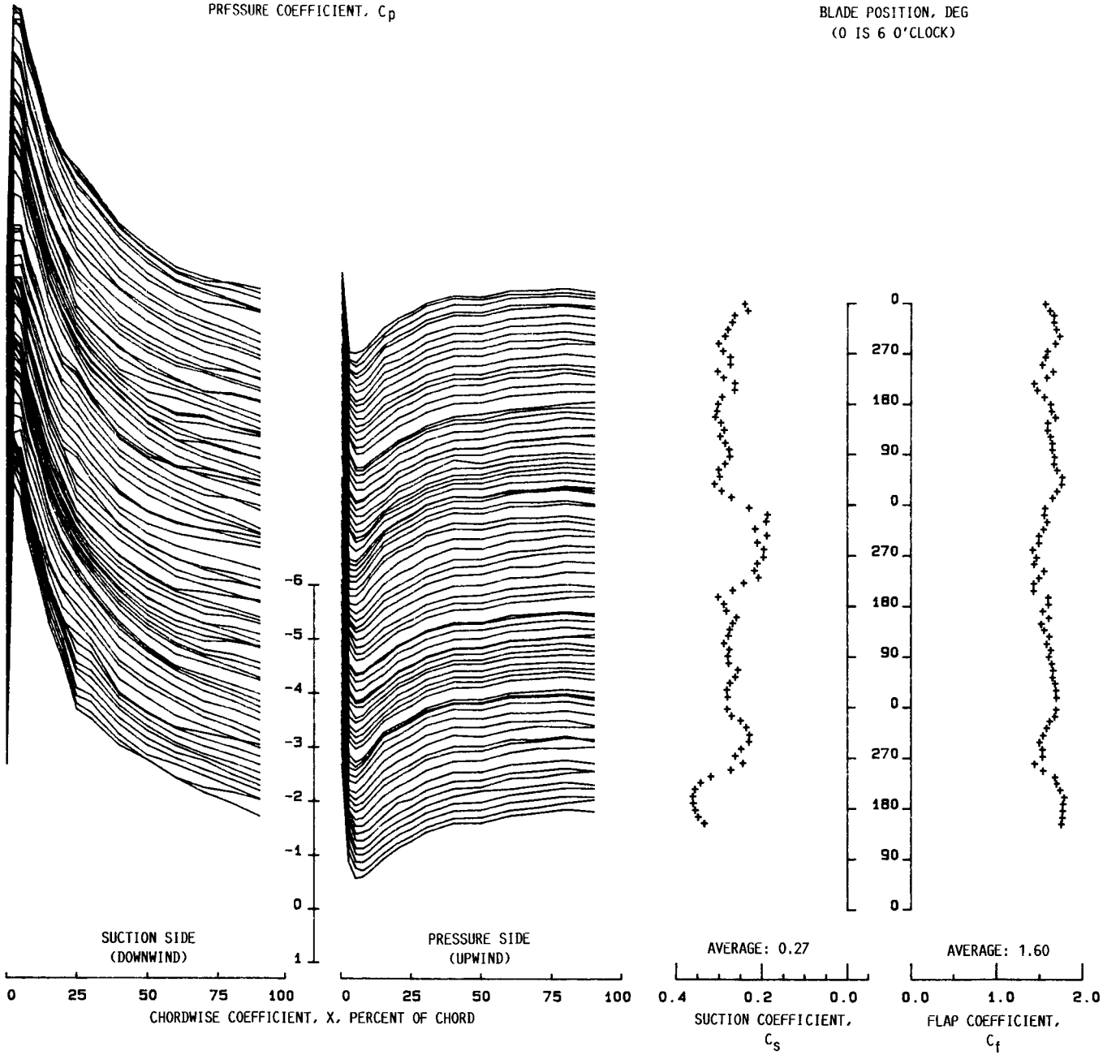

(a) 2680-kW POWER OUTPUT, WITHOUT SEPARATION.

FIGURE 10. - PRESSURE, SUCTION, AND FLAP COEFFICIENTS MEASURED ON MOD-2 WIND TURBINE BLADE WITH VORTEX GENERATORS INSTALLED AND WITH BLADE TIP MOVING TO CONTROL POWER.

ORIGINAL PAGE IS
OF POOR QUALITY

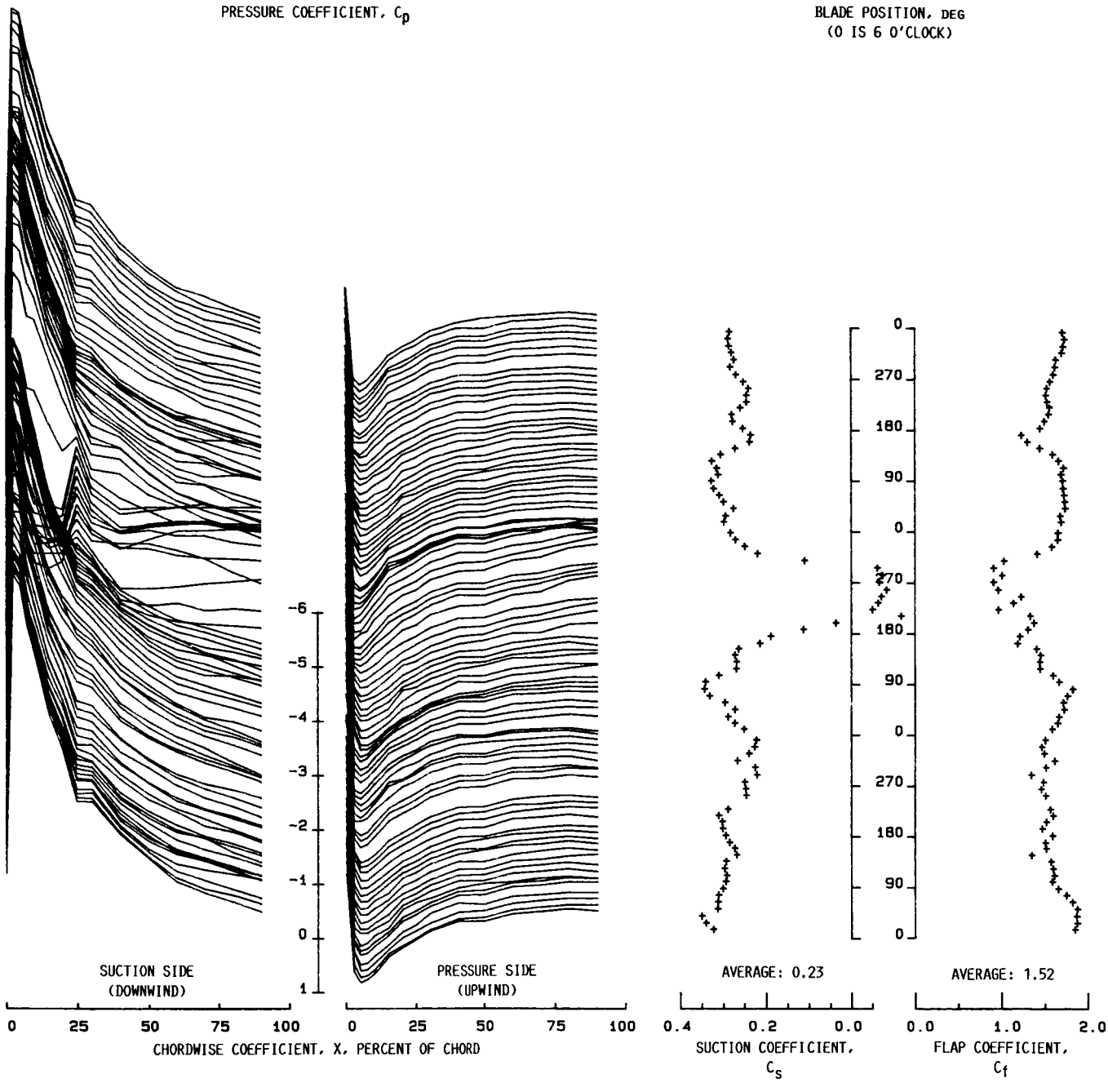

(b) 2680-kW POWER, WITH SEPARATION.

FIGURE 10. - CONCLUDED.

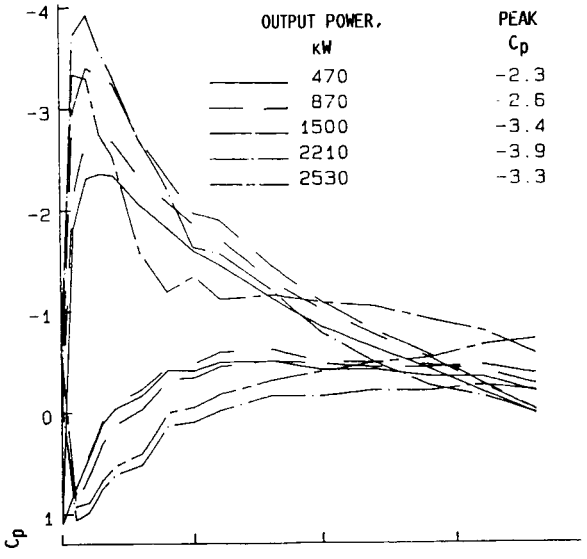

(a) WITHOUT VORTEX GENERATORS.

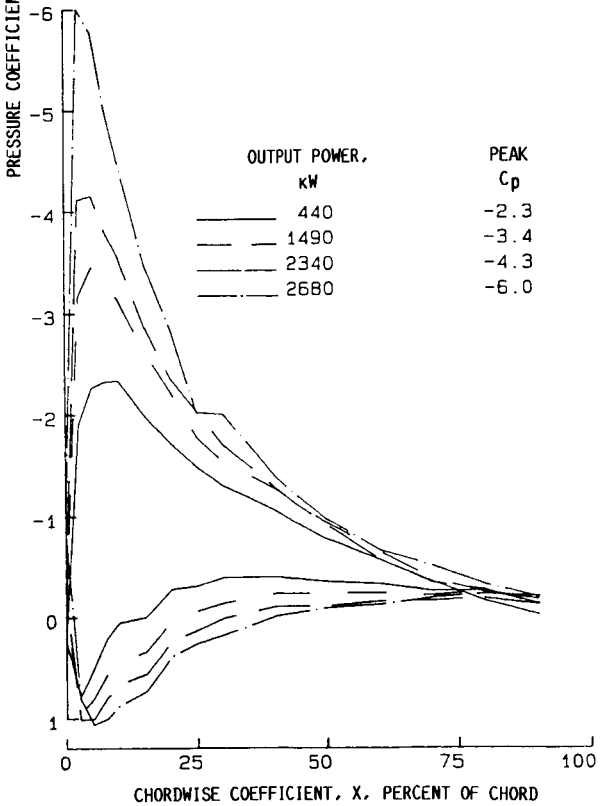

(b) WITH VORTEX GENERATORS INSTALLED.

FIGURE 11. - TYPICAL CHORDWISE DISTRIBUTIONS OF PRESSURE COEFFICIENTS MEASURED ON MOD-2 WIND TURBINE BLADE AT 270° (HORIZONTAL, DESCENDING) POSITION, AT VARIOUS POWER LEVELS.

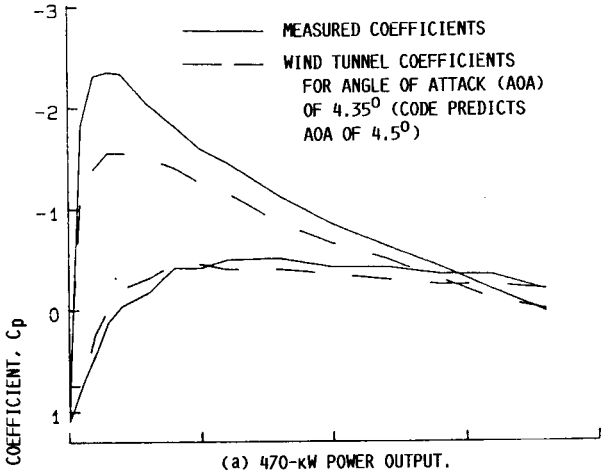

(a) 470-kW POWER OUTPUT.

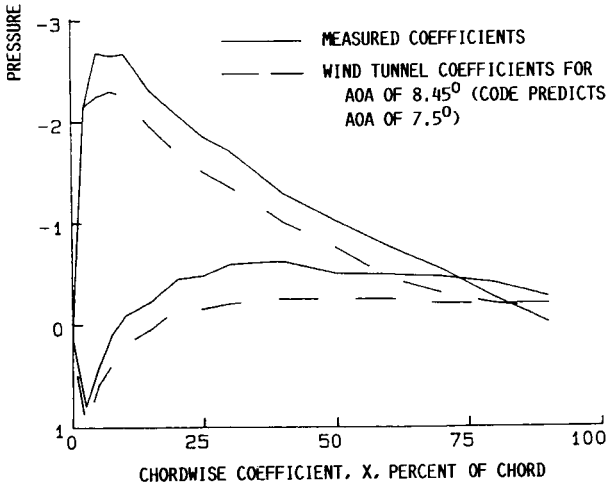

(b) 870-kW POWER OUTPUT.

FIGURE 12. - COMPARISON OF WIND TURBINE AND WIND TUNNEL PRESSURE COEFFICIENTS, WITHOUT VORTEX GENERATORS.

ORIGINAL PAGE IS
OF POOR QUALITY

ORIGINAL PAGE IS
OF POOR QUALITY

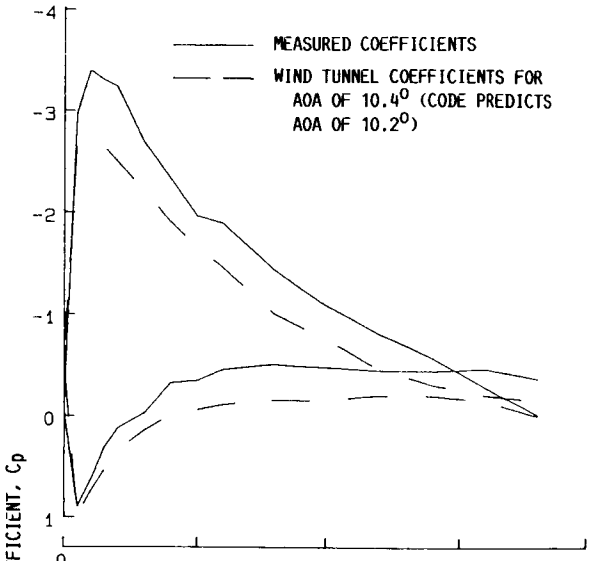

(c) 1500-kW POWER OUTPUT.

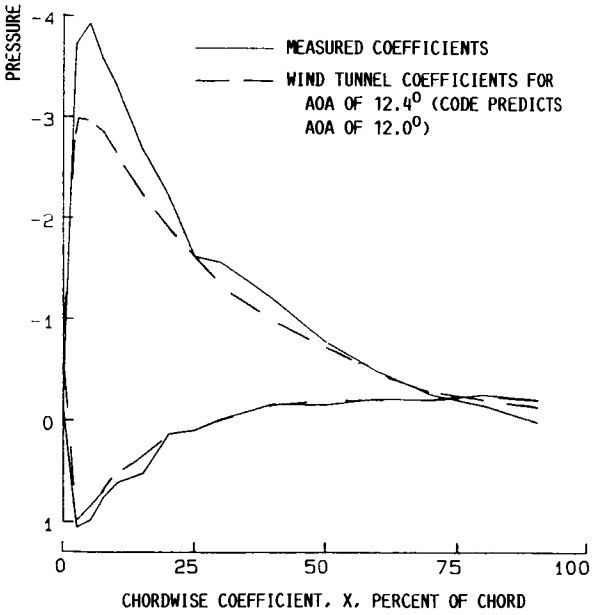

(d) 2210-kW POWER OUTPUT.

FIGURE 12. - CONCLUDED.

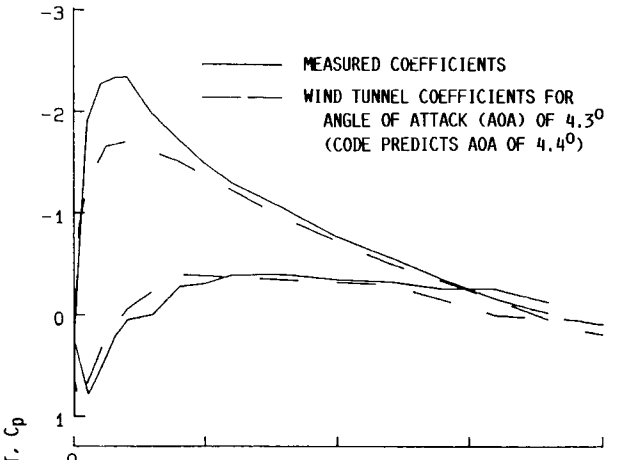

(a) 440-kW POWER OUTPUT.

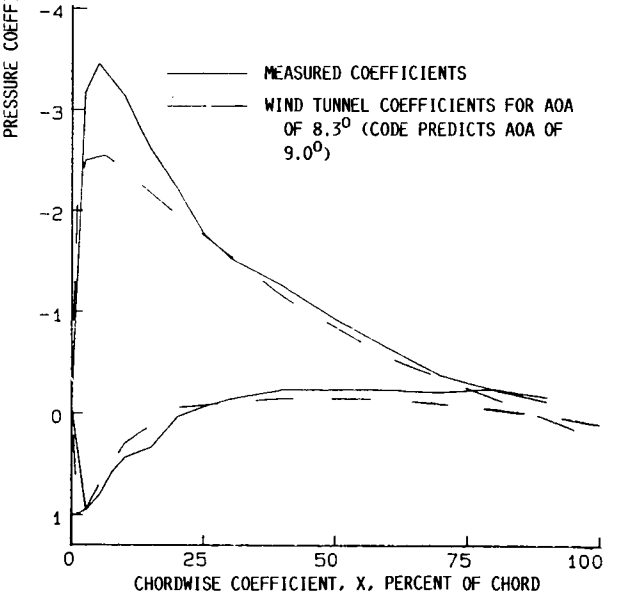

(b) 1490-kW POWER OUTPUT.

FIGURE 13. - COMPARISON OF WIND TURBINE AND WIND TUNNEL PRESSURE COEFFICIENTS WITH VORTEX GENERATORS INSTALLED.

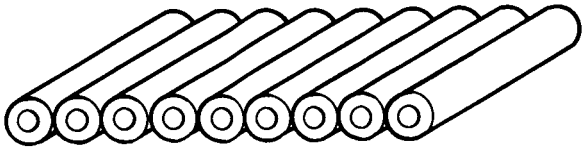

(a) MOLDED RUBBER RIBBON CONTAINING 10 PRESSURE TUBES (3.2-MM O.D., 1.3-MM I.D.).

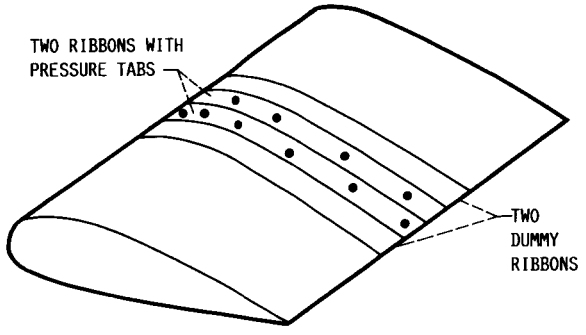

(b) PRESSURE BELT CONSISTING OF FOUR RIBBONS.

FIGURE 14. - CONFIGURATION OF PRESSURE BELT.

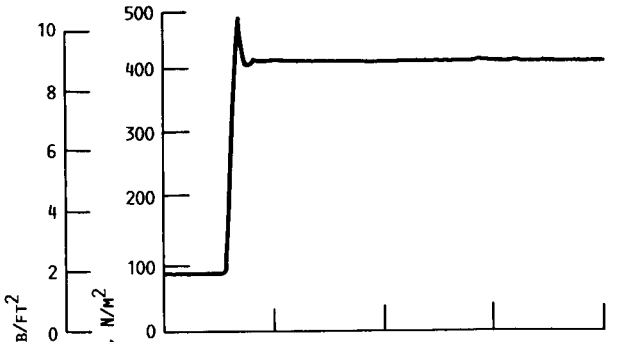

(a) 1.2-M TUBE, SHOWING OVERSHOOT RESPONSE.

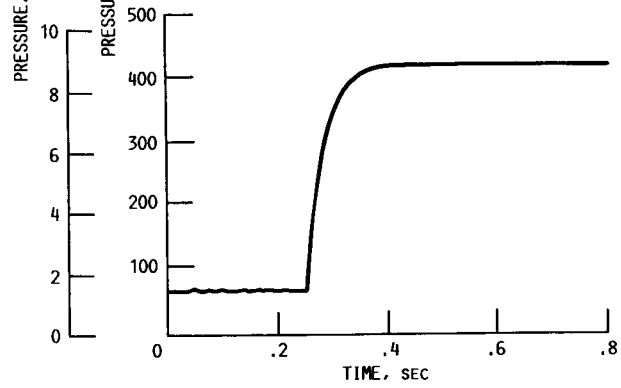

(b) 2.5-M TUBE, SHOWING OVERDAMPED RESPONSE WITH TIME CONSTANT OF APPROXIMATELY 0.025 SEC.

FIGURE 15. - RESPONSE OF PRESSURE TAP/TUBING/SENSOR SYSTEM TO STEP CHANGE IN PRESSURE.

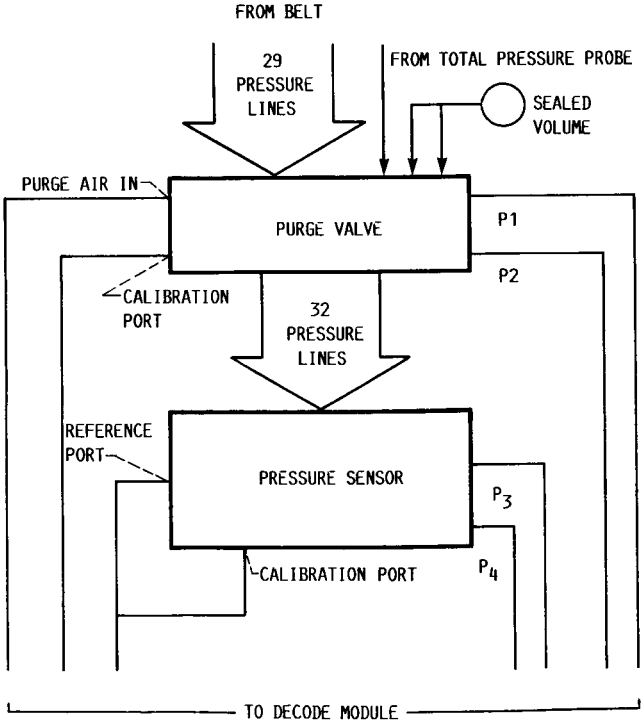

FIGURE 16. - SCHEMATIC DIAGRAM OF PNEUMATIC COMPONENTS MOUNTED ON "D" HATCH.

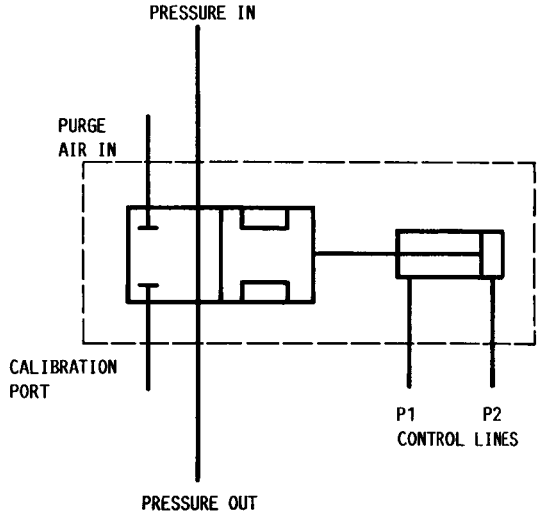

(a) PURGE VALVE (FOUR-WAY SLIDE VALVE).

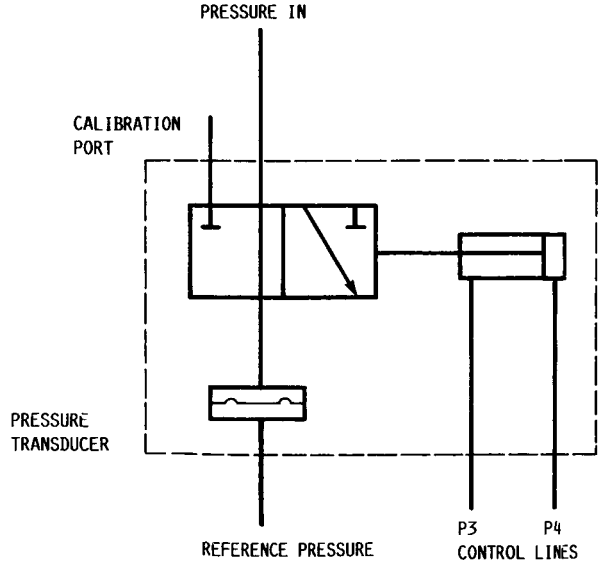

(b) PRESSURE SENSOR (THREE-WAY SLIDE VALVE).

FIGURE 17. - INTERNAL VALVE ARRANGEMENT IN PURGE VALVE AND PRESSURE SENSOR.

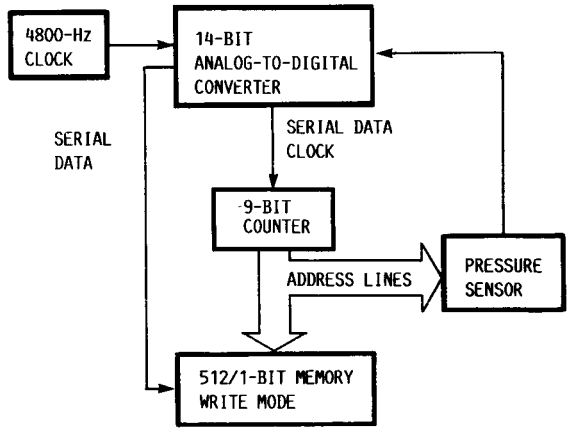

(a) DIGITIZING AND STORAGE MODE.

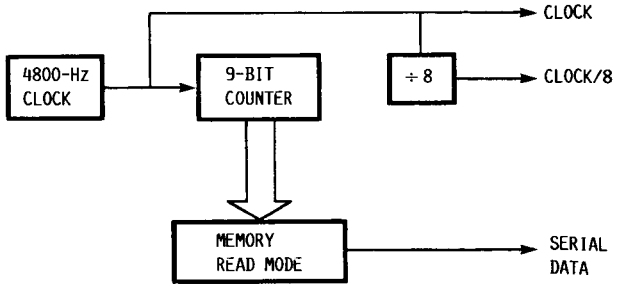

(b) TRANSMIT MODE.

FIGURE 18. - BLOCK DIAGRAM OF SENSOR CONTROL MODULE.

NASA
National Aeronautics and Space Administration

Report Documentation Page

1. Report No.	2. Government Accession No.	3. Recipient's Catalog No.
NASA TM-89903		

4. Title and Subtitle	5. Report Date
Surface Pressure Measurements on the Blade of an Operating Mod-2 Wind Turbine With and Without Vortex Generators	August 1987
	6. Performing Organization Code: 776-33-41
7. Author(s): Ted W. Nyland	8. Performing Organization Report No.: E-3595
	10. Work Unit No.
9. Performing Organization Name and Address: National Aeronautics and Space Administration, Lewis Research Center, Cleveland, Ohio 44135	11. Contract or Grant No.
	13. Type of Report and Period Covered: Technical Memorandum
12. Sponsoring Agency Name and Address: U.S. Department of Energy, Wind/Ocean Technology Division, Washington, D.C. 20545	14. Sponsoring Agency Code: DOE/NASA/20320-72

15. Supplementary Notes

Final Report. Prepared under Interagency Agreement DE-AI01-76ET20320.

16. Abstract

Pressure measurements covering a range of wind velocities were made at one span location on the surface of an operating Mod-2, 2500-kW, wind turbine blade. The data, which were taken with and without vortex generators installed on the leading edge, show the existence of higher pressure coefficients than would be expected from two-dimensional wind tunnel data. These high pressure ratios may be the result of three-dimensional flow over the blade, which delays flow separation. Data are presented showing the repetitiveness of abrupt changes in the pressure distribution that occur as the blade rotates. Calculated values of suction and flap coefficients are also presented.

17. Key Words (Suggested by Author(s))	18. Distribution Statement
Wind turbine; Aerodynamic pressure; Vortex generator; Stall; Transient pressure; Pressure sensor; Pressure instrumentation; Pressure coefficient	Unclassified - unlimited STAR Category 44 DOE Category UC-60

19. Security Classif. (of this report)	20. Security Classif. (of this page)	21. No of pages	22. Price*
Unclassified	Unclassified	34	A03

*For sale by the National Technical Information Service, Springfield, Virginia 22161